Stem Cell Reports
Article

ISSCR

OPEN ACCESS

An Efficient Platform for Astrocyte Differentiation from Human Induced Pluripotent Stem Cells

Julia TCW,[1,2] Minghui Wang,[4,7] Anna A. Pimenova,[1,2,7] Kathryn R. Bowles,[1,2,7] Brigham J. Hartley,[3,7] Emre Lacin,[1,7] Saima I. Machlovi,[1,2] Rawan Abdelaal,[5] Celeste M. Karch,[6] Hemali Phatnani,[5] Paul A. Slesinger,[1] Bin Zhang,[4] Alison M. Goate,[1,2,4,*] and Kristen J. Brennand[1,3,*]

[1]Department of Neuroscience & Friedman Brain Institute, Icahn School of Medicine at Mount Sinai, 1425 Madison Avenue, New York, NY 10029, USA
[2]Ronald M. Loeb Center for Alzheimer's disease, Icahn School of Medicine at Mount Sinai, 1425 Madison Avenue, New York, NY 10029, USA
[3]Department of Psychiatry, Icahn School of Medicine at Mount Sinai, 1425 Madison Avenue, New York, NY 10029, USA
[4]Department of Genetics and Genomic Sciences, Icahn Institute of Genomics and Multiscale Biology, Icahn School of Medicine at Mount Sinai, 1470 Madison Avenue, New York, NY 10029, USA
[5]New York Genome Center, 101 Avenue of the Americas, New York, NY 10013, USA
[6]Department of Psychiatry, Washington University in St. Louis, St. Louis, MO 63130, USA
[7]These authors contributed equally
*Correspondence: alison.goate@mssm.edu (A.M.G.), kristen.brennand@mssm.edu (K.J.B.)
http://dx.doi.org/10.1016/j.stemcr.2017.06.018

SUMMARY

Growing evidence implicates the importance of glia, particularly astrocytes, in neurological and psychiatric diseases. Here, we describe a rapid and robust method for the differentiation of highly pure populations of replicative astrocytes from human induced pluripotent stem cells (hiPSCs), via a neural progenitor cell (NPC) intermediate. We evaluated this protocol across 42 NPC lines (derived from 30 individuals). Transcriptomic analysis demonstrated that hiPSC-astrocytes from four individuals are highly similar to primary human fetal astrocytes and characteristic of a non-reactive state. hiPSC-astrocytes respond to inflammatory stimulants, display phagocytic capacity, and enhance microglial phagocytosis. hiPSC-astrocytes also possess spontaneous calcium transient activity. Our protocol is a reproducible, straightforward (single medium), and rapid (<30 days) method to generate populations of hiPSC-astrocytes that can be used for neuron-astrocyte and microglia-astrocyte co-cultures for the study of neuropsychiatric disorders.

INTRODUCTION

Astrocytes are the most abundant cell type in the CNS, rivaling the diversity of neurons in cellular morphologies, gene expression profiles, developmental origins, physiological properties, functions, and responses to injury and disease (Zhang and Barres, 2010). Within the human brain, astrocytes have a variety of essential functions including glutamate biology, axonal guidance, trophic support, inflammatory response and wound healing, formation of the blood-brain barrier, and neuronal synapse formation, and plasticity (Barres, 2008; Eroglu and Barres, 2010; Freeman and Rowitch, 2013). Although the full contribution of astrocytes to neurological disease remains unresolved, astrocyte cell-autonomous deficits have been implicated in a variety of neurological disorders (Seifert et al., 2006; Tong et al., 2014). The most significant genetic risk factor for Alzheimer's disease (AD), apolipoprotein E4 (*APOE4*), is predominantly synthesized and secreted by astrocytes (Xu et al., 2006). Furthermore, astrocytes derived from human induced pluripotent stem cell (hiPSC)- or mouse-based models of amyotrophic lateral sclerosis (Di Giorgio et al., 2008; Marchetto et al., 2008; Papadeas et al., 2011), Rett syndrome (Ballas et al., 2009), and Huntington disease (Bradford et al., 2009) damage neurons in co-culture or after transplantation.

Evolutionarily, the astrocyte-to-neuron ratio increases from low vertebrates to rodents and to primates (Sherwood et al., 2006). Human cortical astrocytes are larger, structurally more complex and diverse, and propagate calcium waves 4-fold faster than their rodent counterparts (Oberheim et al., 2009). Transplantation of human glia into mice enhances activity-dependent plasticity and learning (Bi et al., 2013). Given the unique biology of human astrocytes, it is critical that improved human-specific cell-based systems be established to enable the study of human astrocyte function in health and disease.

Because of their ability to model all of the (known and unknown) genetic risk factors underlying neuropsychiatric disease, hiPSCs are routinely used as a source of various types of neurons and astrocytes for study (Mertens et al., 2016). Current hiPSC-based methods for the differentiation of astrocytes typically rely on either a neural progenitor cell (NPC) (Haidet-Phillips et al., 2014; Krencik et al., 2011; McGivern et al., 2013; Serio et al., 2013; Shaltouki et al., 2013) or oligodendrocyte progenitor cell (Jiang et al., 2013) intermediate. While it has been widely demonstrated that hiPSCs can be differentiated to functional astrocytes for cell-based models of neuropsychiatric disorders *in vitro* (Haidet-Phillips et al., 2014; McGivern et al., 2013; Serio et al., 2013; Shaltouki et al., 2013) or engraftment *in vivo* (Chen et al., 2015; Haidet-Phillips et al., 2014; Jiang et al., 2013; Krencik et al., 2011), existing methods are slow (up to 6 months) (Jiang et al., 2013; Krencik et al., 2011; Shaltouki et al., 2013) and/or require sorting to reduce

Table 1. Screening Conditions for Astrocyte Differentiation

ID	Reference	Basal Medium	Supplement 1	Supplement 2	Growth Factors			
1	Brennand and Gage (2011)	DMEM/F12	N2, B27	GlutaMAX + sodium bicarbonate + sodium pyruvate	BDNF	GDNF	cAMP	AA
2	ScienCell 1801	ND (AM)	AGS				2% FBS	
3	Thermo Fisher A1261301	DMEM	N2	GlutaMAX + D-glucose + sodium pyruvate			10% FBS	
4	Lonza CC-3186	ND	–	L-glutamine	EGF		3% FBS	insulin + AA
5	C.M.K., unpublished data	neural basal glutamine	2× N2		FGF2 + CNTF			
6	modified from C.M.K., unpublished data	neural basal glutamine	N2, B27	GlutaMAX, NEAA, bME	FGF2 + CNTF			
7	Krencik et al. (2011)	DMEM/F12	N2, B27	GlutaMAX, NEAA, bME	FGF2 + CNTF			
8	Jiang et al. (2013)	DMEM/F12	N2, B27	GlutaMAX, NEAA, bME	FGF2 + CNTF	BMP4		
9	reduction of % FBS from no. 10	DMEM/F12	N2, B27	GlutaMAX, NEAA, bME	FGF2 + CNTF	BMP4	3% FBS	
10	Roybon et al. (2013)	DMEM/F12	N2, B27	GlutaMAX, NEAA, bME	FGF2 + CNTF	BMP4	10% FBS	
11	Shaltouki et al. (2013)	DMEM/F12	N2, B27	GlutaMAX, NEAA, bME	FGF2 + CNTF	BMP4	3% FBS	neuregulin
12	adding insulin + AA to no. 9	DMEM/F12	N2, B27	GlutaMAX, NEAA, bME	FGF2 + CNTF	BMP4	3% FBS	insulin + AA

The 11 screened conditions of astrocyte differentiation from hiPSCs, including 3 commercially available astrocyte media (nos. 2–4) and 8 conditions modified from published protocols (nos. 5–12), with a forebrain neuron differentiation protocol (no. 1). NEAA, non-essential amino acid; bME, 2-mercaptoethanol; AA, ascorbic acid; ND, non-disclosure; AM, astrocyte medium; AGS, astrocyte growth supplement.

heterogeneity (Chaboub and Deneen, 2013; Yuan et al., 2011). Here, we screened a number of published protocols, along with commercially available media for primary human astrocyte culture, identifying a robust and straightforward differentiation protocol for generating astrocytes from hiPSCs. By co-culture with microglia, we compared the function of primary human fetal astrocytes and hiPSC-astrocytes in assays for neuroinflammatory response, phagocytosis, and spontaneous calcium activity, concluding that hiPSC-astrocytes are highly similar to their primary counterparts. Altogether, our rapid differentiation protocol, co-culture strategy, and scalable phenotypic assays will serve as a robust platform for queries of healthy and diseased human astrocytes.

RESULTS

30-Day Exposure of hiPSC-Derived NPCs to Commercial Astrocyte Media Is Sufficient to Robustly Generate hiPSC-Astrocytes

We first screened 11 different media conditions on forebrain-patterned NPCs (Brennand et al., 2015; Brennand and Gage, 2011) derived from hiPSCs (Table 1). The screening conditions, based on recently published hiPSC-astrocyte differentiation protocols (Chen et al., 2015; Haidet-Phillips et al., 2014; Jiang et al., 2013; Krencik et al., 2011; McGivern et al., 2013; Serio et al., 2013; Shaltouki et al., 2013), included different combinations of fibroblast growth factor 2 (FGF2) (Haidet-Phillips et al., 2014), ciliary neurotrophic factor (CNTF), (Krencik et al., 2011; Shaltouki et al., 2013), bone morphogenetic protein 4 (BMP4) (Han et al., 2013; Jiang et al., 2013; Shaltouki et al., 2013), fibroblast bovine serum (FBS) (Han et al., 2013; Shaltouki et al., 2013), neuregulin (Pinkas-Kramarski et al., 1994; Shaltouki et al., 2013), insulin (Heni et al., 2011), and ascorbic acid (AA) (Palm et al., 2015), as well as three commercial astrocyte media (ScienCell, Gibco, and Lonza) for the culture of primary human fetal astrocytes (Table 1). Screening criteria included immunoreactivity for two classical markers of astrocyte identity, S100β and glial fibrillary acidic protein (GFAP) (Ludwin et al., 1976), astrocyte morphology, survival, replicative ability, and cell line variability (Table S1; Figure S1A). When tested on NPCs, most conditions resulted in limited cell proliferation and expression of neuronal markers (Table S1); however,

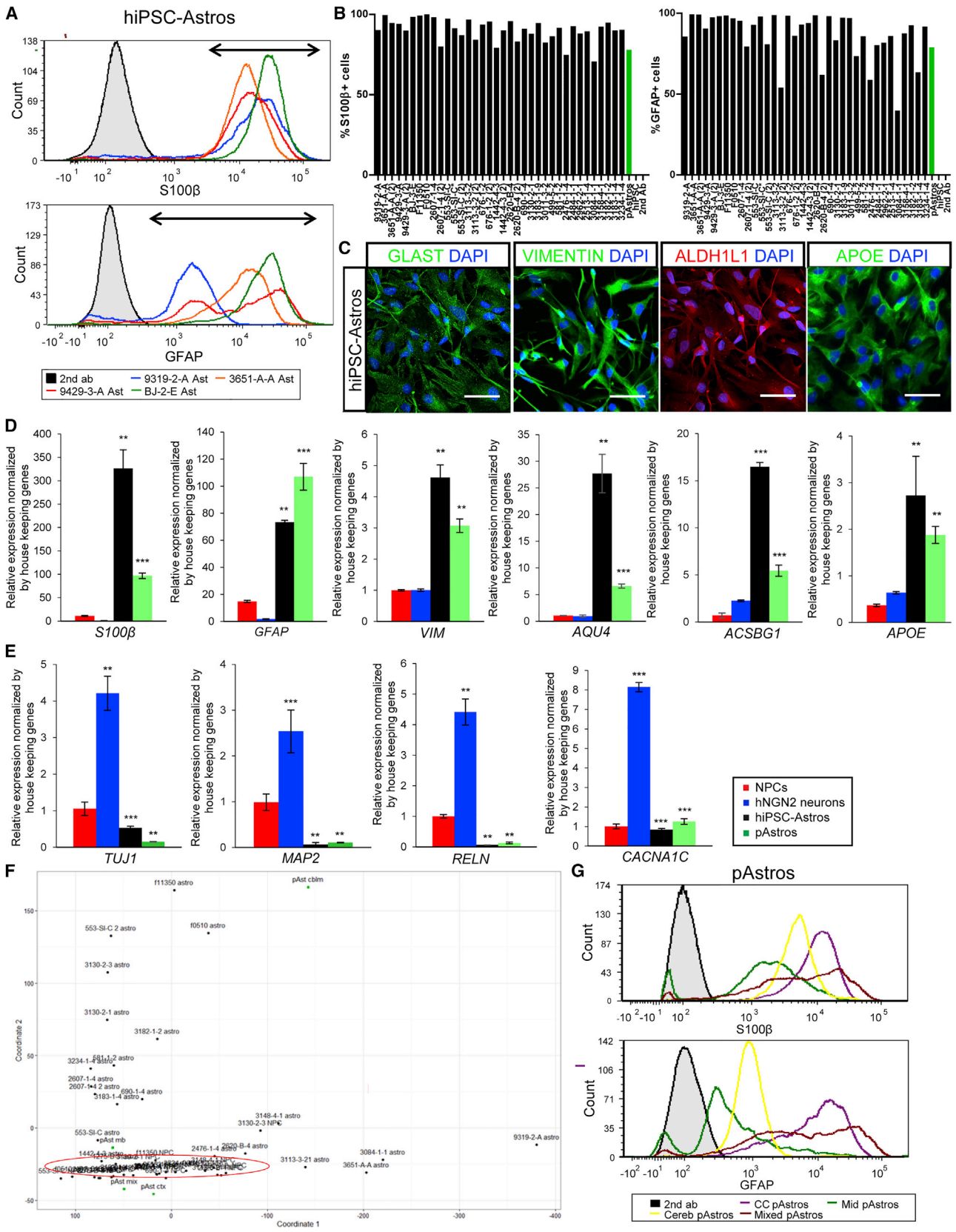

(legend on next page)

two commercial media, ScienCell and Lonza, yielded S100β- and GFAP-positive astrocyte-like cells (Figures S1B–S1D). These results were confirmed across four representative NPC lines by both flow cytometry and immunocytochemistry by 30 days (Figures 1A and S1E–S1G). Culture of NPCs in both media, when combined with low initial seeding density (nearly single cells: 15,000 cells/cm^2) and minimal serum exposure (1%–2%), resulted in astrocyte morphology within 10 days (Figure S1H); star-shaped astrocyte morphologies were evident within 30 days (Figure S1I). Although ScienCell and Lonza astrocyte media showed equivalent efficiencies (Figures S1B–S1D), ScienCell medium was selected owing to its lower cost and relative simplicity.

We next tested the efficacy of this protocol across 42 NPC lines from 30 individuals (including healthy controls as well as cases with schizophrenia and frontotemporal dementia; 16 male and 14 female) generated as part of three unique hiPSC cohorts (reprogrammed and differentiated through different protocols in independent laboratories) (Table S2). All 42 NPC lines ultimately yielded replicative cells with an astrocyte-like morphology (although not necessarily on the first attempt), with an average composition of 90% S100β$^+$ and 82% GFAP$^+$ cells by flow cytometry, relative to the appropriate secondary antibody control (Figures 1A and 1B; hiPSCs served as a negative control, lacking S100β- and GFAP-positive cells), and confirmed by immunocytochemistry (Figures 1A, 1C, S1J, and S1K). As with primary astrocytes (Figures 1G and S1O), there is substantial variability in mean fluorescent intensity between S100β- and GFAP-positive hiPSC-astrocyte populations (Figure 1A).

Within 30 days, hiPSC-astrocytes were immunopositive for the astrocyte markers ALDH1L1 (Cahoy et al., 2008) and Vimentin (VIM) (Schnitzer et al., 1981), as well as the glutamate transporters GLAST (EAAT1 and GLUT1) (Rothstein et al., 1994) (Figures 1C, S1L, and S1M). Compared with NPCs or excitatory neurons (h*NGN2*-induced neurons) (Brennand et al., 2015), hiPSC-astrocytes expressed *GFAP* (Ludwin et al., 1976), *S100β* (Ludwin et al., 1976), *VIM* (Schnitzer et al., 1981), *AQU4* (Hubbard et al., 2015), *ACSBG1* (Chaboub and Deneen, 2013), and *APOE* (Boyles et al., 1985) by qPCR (Figure 1D), although expression levels between individual hiPSC-astrocytes and primary astrocyte lines varied substantially. In addition, hiPSC-astrocytes expressed low levels of the neuronal markers *TUJ1*, *MAP2AB*, *RELN*, and *CACNA1C* (Figure 1E).

Across a larger panel of neural lineage markers (Table S4) in 23 hiPSC-astrocyte lines and their isogenic NPC lines, principal component analysis (PCA) revealed that the NPCs grouped together, while the astrocytes (both hiPSC-derived and primary human fetal astrocytes) were more dispersed (Figures 1F and S1N). Because it was apparent in our hiPSC-astrocytes as well as the primary human fetal astrocytes (obtained from different donors and brain regions), this variability in lineage marker expression may reflect inter-individual variability and/or differences in regional patterning (Figures 1G and S1O).

hiPSC-Astrocytes and Primary Human Fetal Astrocytes Share Similar Transcriptional Profiles

To query the extent to which global gene expression in hiPSC-astrocytes resembles primary human fetal brain astrocytes, we performed RNA sequencing (RNA-seq) transcriptomic analyses on four control hiPSC-astrocytes and primary human fetal astrocytes from two brain regions (cerebral cortex and midbrain), together with isogenic

Figure 1. Rapid Differentiation of hiPSC-Derived NPCs to Astrocyte-like Identity

(A) Representative flow-cytometry analysis of S100β (top) and GFAP (bottom) for four 30-day hiPSC-astrocyte differentiations. Arrows indicate the cells positive for each marker protein. Appropriate secondary-only control is shown in black.

(B) Graphs of flow-cytometry analysis across 35 hiPSC-astrocyte differentiations from 26 NPC lines from three independent hiPSC cohorts. S100β (left) and GFAP (right) immunostaining is shown, with primary human fetal astrocytes (positive control) and hiPSCs (negative control).

(C) Representative immunofluorescence images of hiPSC-astrocytes stained for astrocyte markers, glutamate transporters GLAST (green), VIMENTIN (green), ALDH1L1 (red), and APOE (green). Scale bars, 100 μm.

(D) mRNA levels of astrocyte markers: *S100β*, *GFAP*, *VIM*, *AQU4*, *ACSBG1*, and *APOE* in hiPSC-astrocytes (n = 3 from four different lines) and primary human fetal astrocytes (pAstrocytes; n = 3 from cerebral cortex astrocytes). Primer sequences are listed in Table S3. n, the number of independent experiments.

(E) mRNA levels of neuronal markers: *TUJ1*, *MAP2AB*, *RELN*, and *CACNA1C* in hiPSC-astrocytes (n = 3 from four different lines) and pAstrocytes (n = 3 from cerebral cortex astrocytes), relative to h*NGN2*-induced neurons (n = 3 from two lines). Primer sequences are listed in Table S3.

(F) Principal component analysis of lineage-specific marker expression in 23 pairs of hiPSC-astrocytes and isogenic source NPCs, together with four pAstrocyte lines isolated from fetal cerebral cortex, midbrain, cerebellum, and whole brain.

(G) Flow-cytometry analysis of S100β (top) and GFAP (bottom) for pAstrocytes from the cerebral cortex, midbrain, cerebellum, and whole brain. Appropriate secondary-only control is shown in black. CC, cerebral cortex; Mid, midbrain; Cereb, cerebellum; Mixed, whole brain; hiPSC-Astros, hiPSC-astrocytes; pAstros, primary human fetal astrocytes.

Data are presented as mean ± SD using two-tailed homoscedastic Student's t test. $^{**}p < 0.01$, $^{***}p < 0.001$.

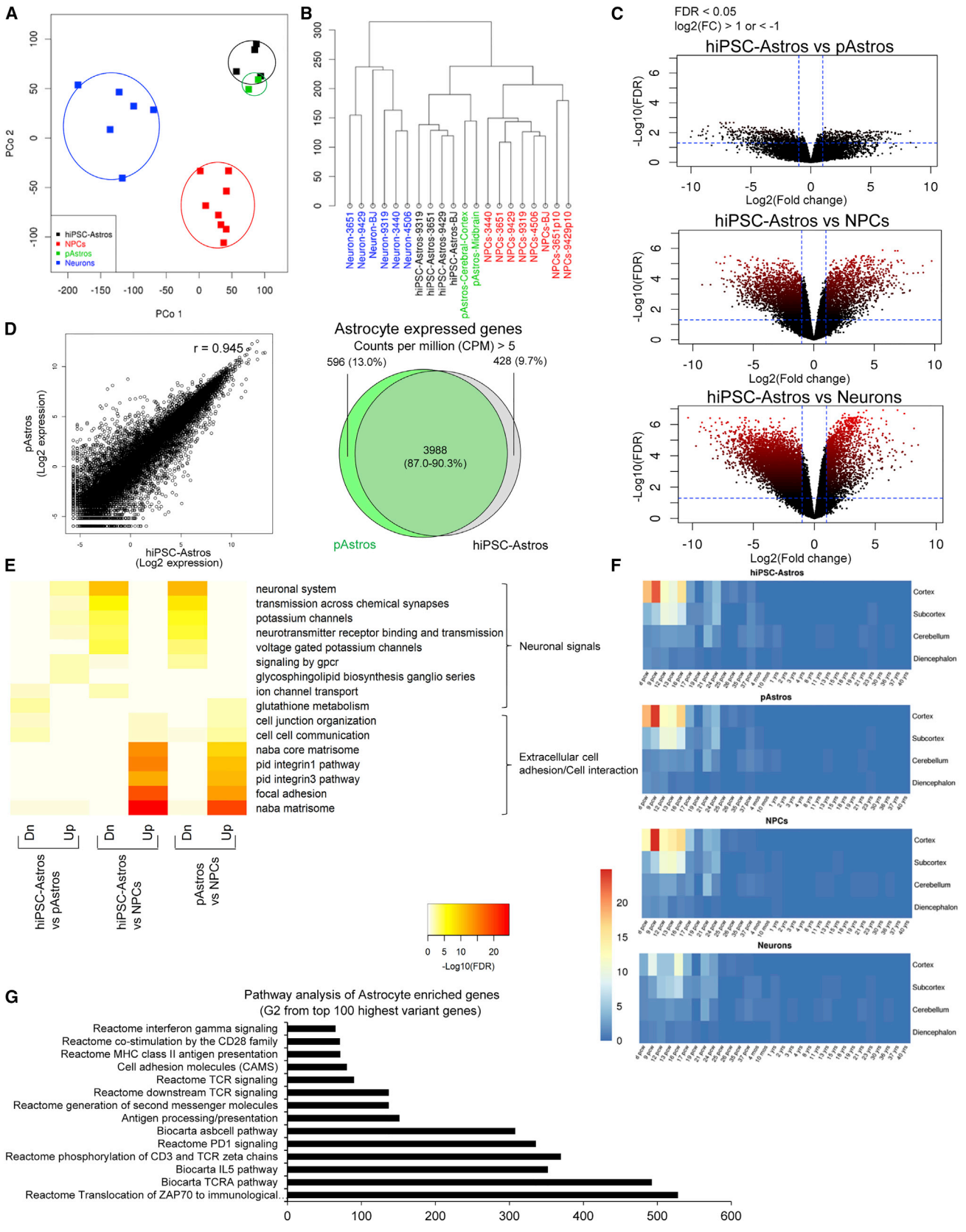

(legend on next page)

hiPSC-derived NPCs and neurons (Figures 2 and S2), comparing them with *in vivo* human and rodent astrocyte transcriptomic datasets (Figures 2, 3, S2, and S3). hiPSC-astrocytes showed transcriptional profiles most similar to those of fetal brain astrocytes. Using PCA and hierarchical clustering, all four hiPSC-astrocytes clustered together with the primary human fetal astrocytes and distinct from the NPC and neuron clusters (Figures 2A, 2B, and S2A).

There were nearly 6-fold fewer differentially expressed genes (DEGs) between hiPSC-astrocytes and primary human fetal astrocytes (900 genes) than between hiPSC-astrocytes and isogenic hiPSC-derived neurons (10,000 genes) or NPCs (5,500 genes) (Figures 2C and S2B). hiPSC-astrocytes are highly similar to primary human fetal astrocytes ($r = 0.945$); the majority of both expressed genes (counts per million [CPM] > 1) and enriched genes (CPM > 5) were shared between hiPSC-astrocytes and primary human fetal astrocytes (87.0% and 90.3%, respectively) (Figure 2D). Functional enrichment analyses (using MSigDB) demonstrated that signals regulating neuronal maturation, such as synapse or ion channel formation, were downregulated in hiPSC-astrocytes and primary human fetal astrocytes, whereas signals promoting extracellular cell adhesion and interaction were upregulated (Figure 2E). When we specifically considered just the top 100 most varying genes distinguishing hiPSC-astrocytes from hiPSC-derived NPCs and neurons, functional enrichment analysis identified a group of 19 genes related to reactivity, cytokine, interferon, T cell receptor (TCR), and antigen-processing signaling that were enriched in astrocytes (G2) (Figures 3A and S2C; Table 2).

To assess the extent to which hiPSC-astrocytes are related to human brain astrocytes *in vivo*, we compared expression profiles of hiPSC-derived astrocytes, NPCs, and neurons from four healthy controls, as well as primary human fetal astrocytes, with the Allen BrainSpan Atlas of the Developing Human Brain (http://www.brainspan.org) (Miller et al., 2014) using a Spearman rank correlation analysis. Heatmaps generated through a Wilcoxon's rank-sum test revealed that gene expression in hiPSC-astrocytes and primary human fetal astrocytes was highly correlated with gene expression in human fetal cortical brain tissue (8–16 weeks post conception) (Figure 2F). Unsupervised hierarchical cell-type-specific cluster analysis demonstrated that hiPSC-astrocytes closely cluster with astrocytes purified by immunopanning from human brain tissue, particularly hippocampal astrocytes, rather than oligodendrocytes, endothelial cells, myeloid cells, or neurons (Zhang et al., 2016) (Figure 3A); pathway analysis further revealed that many astrocyte-enriched genes were related to immune signaling (Figure 2G).

Expression Profile of hiPSC-Astrocytes Resembles Quiescent Astrocytes

To determine whether the gene expression pattern of our control hiPSC-astrocytes more resembles quiescent or reactive astrocytes, we compared them with an RNA-seq dataset of "proinflammatory" A1-type and "immunoregulatory" A2-type murine astrocytes, as well as their saline- and sham-treated controls (Zamanian et al., 2012). (Because these are *in vivo* cell types, whereby A1-type astrocytes are induced by a bacterial lipopolysaccharide [LPS] infection and A2-type astrocytes by middle cerebral artery occlusion [MCAO], no comparable dataset exists for human astrocytes.) hiPSC-astrocyte gene expression best clusters with the control conditions (Figures 3B and S3A), suggesting that hiPSC-astrocytes may be closer to the quiescent state than to reactive astrocytes.

Figure 2. Transcriptional Profile of hiPSC-Astrocytes and Primary Human Fetal Astrocytes

RNA-seq analysis of hiPSC-derived NPCs (n = 8), neurons (n = 6), and astrocytes (n = 4) together with pAstrocytes from human fetal cerebral cortex and midbrain.

(A and B) Principal component (P.Co) analysis (A) and clustering diagram (B) of hiPSC-derived NPCs, neurons, and astrocytes, together with pAstrocytes.

(C) Volcano plot comparison of hiPSC-astrocytes to pAstrocytes (top), as well as to hiPSC-derived NPCs (middle) and neurons (bottom). Average $\log_2$(fold change) versus $-\log_{10}$(FDR) is shown for all genes. Genes upregulated and downregulated by 2-fold change and FDR < 0.05 are labeled by red dots. The number of genes differentially expressed between different cell types is indicated by the red color density and quantified in Figure S2B.

(D) Scatterplot (left) comparing gene expression in hiPSC-astrocytes and pAstrocytes. r represents the Spearman correlation coefficient. Venn diagram (right) of overlapping gene expression (CPM > 5) between hiPSC-astrocytes and pAstrocytes.

(E) Functional pathway enrichment analysis of differentially expressed genes between hiPSC-astrocytes and pAstrocytes (left), hiPSC-astrocytes and NPCs (middle), and pAstrocytes and NPCs (right); hiPSC-astrocytes and pAstrocytes express increased extracellular cell communication signals, but decreased neuronal signals relative to NPCs.

(F) Heatmap produced by Wilcoxon's rank-sum comparisons of hiPSC-derived NPCs, neurons, and astrocytes, as well as pAstrocytes, relative to the Allen BrainSpan Atlas.

(G) Fold enrichment from functional pathway analysis of astrocyte-enriched genes, group G2 sorted from top 100 most variable genes from Figure S3A and Table 2.

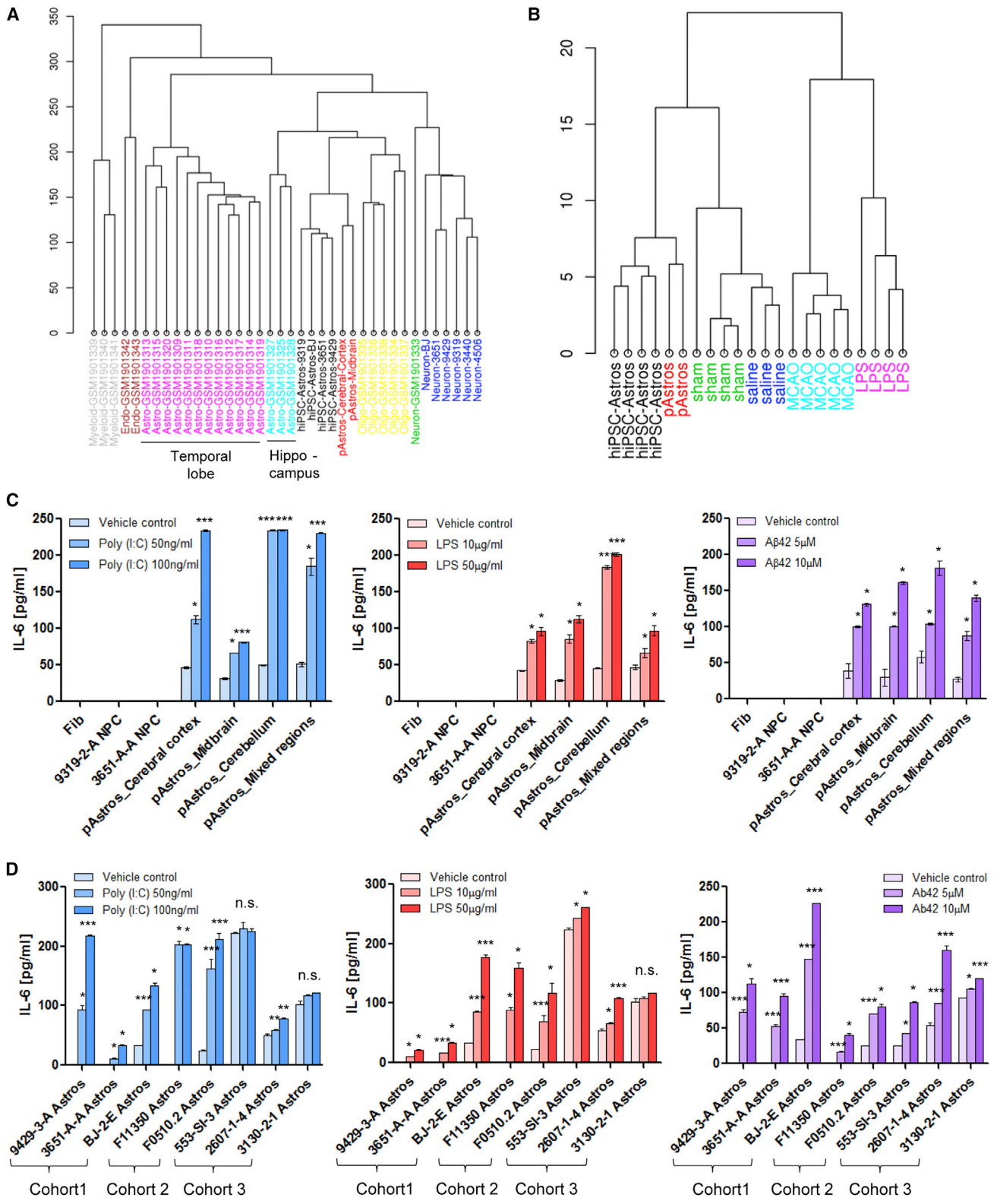

(legend on next page)

hiPSC-Astrocytes Secrete Cytokines in Response to Inflammatory Stimuli

A key effector of the astrocyte neuroinflammatory response in neurodegenerative diseases is interleukin 6 (IL-6) (Zhao and Schwartz, 1998). Consistent with effects observed in primary human fetal astrocytes (Figure 3C), 24-hr treatment with polyinosinic-polycytidylic acid (poly(I:C)) (50 ng/mL or 100 ng/mL), LPS (10 μg/mL or 50 μg/mL), and β-amyloid 42 (Aβ42) (5 μM or 10 μM) led to dose-dependent increases in IL-6 secretion in control hiPSC-astrocytes (Figure 3D), but not the source hiPSC-derived NPCs (Figure 3C).

To more fully characterize the release of inflammatory mediators from control hiPSC-astrocytes following 24-hr treatment with 5 μM Aβ42, a main component of the amyloid plaques in AD, we measured proinflammatory (IL-1β, IL-4, IL-6, IL-8, IL-10, and tumor necrosis factor α) and anti-inflammatory cytokines (IL-1α, IL-2, IL-12, IL-17α, interferon-γ, and granulocyte macrophage colony-stimulating factor) by Multi-Analyte ELISArray, confirming that Aβ42 treatment primarily increased IL-6 secretion (Garwood et al., 2011), as well as a second proinflammatory cytokine, IL-8 (Figures S3B and S3C). We also measured 36 cytokines, chemokines, and acute-phase proteins using the Proteome Profiler Human Cytokine Array (Table S5) in baseline conditions and following 24-hr treatment with 5 μM Aβ42 (Figures 3D and S3C–S3E); Aβ42 increased IL-6 release in both hiPSC-astrocytes and primary human fetal astrocytes (Figure S3D). Together, our findings indicate that hiPSC-astrocytes are capable of secreting proinflammatory cytokines in response to neuroinflammatory cues.

hiPSC-Astrocytes Display Phagocytic Capacity and Promote Phagocytic Function of Microglia

Astrocytes can phagocytose and degrade β-amyloid in AD (Chung et al., 2013; Wyss-Coray et al., 2003). We used flow cytometry to examine the ability of control hiPSC-astrocytes to phagocytose pHrodo red conjugated myelin or zymosan bioparticles (pHrodo red dye fluoresces red in the acidic environment of phagosomes; zymosan is an agonist of Toll-like receptor 2 [TLR2] [Marinelli et al., 2015; Richard et al., 2008]). hiPSC-astrocytes, primary human fetal astrocytes, and BV2 microglia showed a similar capacity to internalize myelin purified from brain homogenates, while zymosan bioparticle uptake was much greater in microglia (consistent with higher levels of TLR2 reported in microglia) (Jana et al., 2008) (Figures 4A, 4B, and S4A–S4C; Movies S1–S3). The specificity of bioparticle uptake was confirmed by treating cells with cytochalasin D, an inhibitor of β-actin polymerization that reduces phagocytosis (Figures 4A and 4B).

Although microglia are the major phagocytic cells in the brain, astrocytes mediate microglial response to inflammatory stimuli (Krencik et al., 2011; Lee and Landreth, 2010; Skripuletz et al., 2013). We repeated the pHrodo red zymosan assay using microglia-astrocyte co-cultures; both hiPSC-astrocytes and primary human fetal astrocytes enhanced phagocytic capacity of BV2 mouse microglial cells (Figures 4C and S4D). We discriminated microglia and astrocyte phagocytic activity by labeling CD11b- and GFAP-positive cells, respectively (Figure S4E). After 3 hr of labeling, only the $CD11b^+$ BV2 microglial cells phagocytosed the pHrodo red zymosan bioparticles (Figure S4E) Finally, we treated BV2 microglial cells with astrocyte conditioned medium (ACM) for 24 hr prior to analyzing their phagocytic capacity; pretreatment of BV2 microglial cells with ACM from either hiPSC-astrocytes or primary human fetal astrocytes significantly increased microglial phagocytic capacity (Figures 4D and S4F). Taken together, these findings show that both hiPSC-astrocytes and primary human fetal astrocytes secrete factors that increase the capacity of microglia to phagocytose zymosan bioparticles.

hiPSC-Astrocytes Display Spontaneous Calcium Transient Activity

We next evaluated whether control hiPSC-astrocytes exhibit spontaneous calcium transients, as has been

Figure 3. Characterization of the Neuroinflammatory Status and Reactivity of hiPSC-Astrocytes

(A) Cluster analysis of hiPSC-derived NPCs, neurons, and astrocytes, as well as pAstrocytes, combined with a human adult brain dataset (Zhang et al., 2016). hiPSC-Astros, hiPSC-astrocytes; pAstros, primary human fetal astrocytes; FDR, false discovery rate; CPM, counts per million.

(B) Cluster diagram of hiPSC-astrocytes and pAstrocytes compared with the astrocyte reactivity dataset (Zamanian et al., 2012), which was sorted by reactivity genes enriched in the A1 (LPS-treatment), A2 (MCAO ischemia), and pan-reactive phenotypes, or related controls (saline and sham, respectively).

(C) IL-6 secretion from pAstrocytes (cerebral cortex, midbrain, cerebellum and whole brain [mixed regions]) and negative controls (fibroblasts and NPCs), after 24-hr treatment with 50 ng/mL or 100 ng/mL poly(I:C), 10 μg/mL or 50 μg/mL LPS, or 5 μM or 10 μM Aβ42 and its relative vehicle controls (saline for poly(I:C) and LPS, and Tris-HCl [pH 8] for Aβ(1–42)), as measured by ELISA.

(D) IL-6 secretion following 24-hr treatment with poly(I:C), LPS, and Aβ42 across hiPSC-astrocyte differentiations from nine NPC lines from three independent hiPSC cohorts. hiPSC-Astros, hiPSC-astrocytes; pAstros, primary human fetal astrocytes.

Data are presented as mean ± SD using one-way ANOVA with Tukey multiple comparison test. n.s., not significant; $*p < 0.05$, $***p < 0.001$.

Table 2. Annotation of the Top 100 Most Variable Genes

MSigDB	Group	Overlap Size	Group Size	MSigDB Size	FE	p Value	FDR	Overlap Genes
Antigen processing and presentation	G2	7	19	57	151.3	1.71×10^{-14}	8.49×10^{-11}	CD74; HLA-DOA; HLA-DQA1; HLA-DQB1; HLA-DRA; HLA-DRB1; HLA-DRB5
Cell adhesion molecules (CAMS)	G2	6	19	115	64.3	3.17×10^{-10}	3.61×10^{-7}	HLA-DOA; HLA-DQA1; HLA-DQB1; HLA-DRA; HLA-DRB1; HLA-DRB5
Reactome MHC class II antigen presentation	G2	5	19	86	71.6	6.64×10^{-9}	6.94×10^{-6}	CD74; HLA-DOA; HLA-DQA1; HLA-DRB1; HLA-DRB5
Reactome translocation of ZAP70 to immunological synapse	G2	3	19	7	528	1.58×10^{-8}	1.53×10^{-5}	HLA-DQA1; HLA-DRB1; HLA-DRB5
Reactome phosphorylation of CD3 and TCR ζ chains	G2	3	19	10	369.6	5.42×10^{-8}	4.85×10^{-5}	HLA-DQA1; HLA-DRB1; HLA-DRB5
Reactome PD1 signaling	G2	3	19	11	336	7.45×10^{-8}	6.22×10^{-5}	HLA-DQA1; HLA-DRB1; HLA-DRB5
Reactome generation of second messenger molecules	G2	3	19	18	205.3	3.67×10^{-7}	0.000287	HLA-DQA1; HLA-DRB1; HLA-DRB5
Reactome downstream TCR signaling	G2	3	19	27	136.9	1.31×10^{-6}	0.000965	HLA-DQA1; HLA-DRB1; HLA-DRB5
Neuron differentiation	G1	4	28	73	45.8	1.68×10^{-6}	0.001205	CNTN4; LMX1B; OTX2; SLIT1
Generation of neurons	G1	4	28	79	42.3	2.31×10^{-6}	0.001574	CNTN4; LMX1B; OTX2; SLIT1
Axon guidance	G1	3	28	22	114	2.32×10^{-6}	0.001574	CNTN4; OTX2; SLIT1
Neurogenesis	G1	4	28	89	37.6	3.73×10^{-6}	0.002458	CNTN4; LMX1B; OTX2; SLIT1
Nervous system development	G1	6	28	366	13.7	3.95×10^{-6}	0.002538	CNTN4; LMX1B; LY6H; OTX2; SHOX2; SLIT1
Reactome TCR signaling	G2	3	19	41	90.1	4.74×10^{-6}	0.002876	HLA-DQA1; HLA-DRB1; HLA-DRB5
Nervous system development	S1	5	17	366	18.8	4.82×10^{-6}	0.002876	CNTN4; LMX1B; LY6H; SHOX2; SLIT1
Biocarta TCRA pathway	G2	2	19	5	492.8	6.23×10^{-6}	0.003549	HLA-DRA; HLA-DRB1
Reactome co-stimulation by the CD28 family	G2	3	19	52	71.1	9.77×10^{-6}	0.005322	HLA-DQA1; HLA-DRB1; HLA-DRB5
Reactome interferon-γ signaling	G2	3	19	57	64.8	1.29×10^{-5}	0.006553	HLA-DQA1; HLA-DRB1; HLA-DRB5
Biocarta IL-5 pathway	G2	2	19	7	352	1.31×10^{-5}	0.006553	HLA-DRA; HLA-DRB1
Axonogenesis	G1	3	28	42	59.7	1.71×10^{-5}	0.007939	CNTN4; OTX2; SLIT1
Biocarta asbcell pathway	G2	2	19	8	308	1.74×10^{-5}	0.007939	HLA-DRA; HLA-DRB1
Neuron differentiation	S1	3	17	73	56.6	1.92×10^{-5}	0.00858	CNTN4; LMX1B; SLIT1

MSigDB (http://software.broadinstitute.org/gsea/msigdb) is a collection of gene annotations, including gene ontology, and functional pathways. Overlap size: the number of genes shared between a query gene set (e.g., genes in group 1, G1) and a gene set in MSigDB (e.g., antigen processing and presentation). Group size: the number of genes in a query gene set. MSigDB size: the number of genes in MSigDB gene set. FE, fold enrichment; FDR, false discovery rate.

described for astrocytes (Volterra et al., 2014). We used the calcium indicator Fluo-4AM to monitor calcium signaling under basal conditions and in response to a pulse of extracellular glutamate (3 μM) (Zhang et al., 2016). A single pulse of glutamate produced a slow calcium response in both hiPSC-astrocytes and primary human fetal astrocytes (Figure 5). In addition, some cells exhibited spontaneous calcium spikes, suggesting the presence of a network of connected astrocytes (Scemes and Giaume, 2006) (Figures 5A–5D). To quantify these responses, we measured the

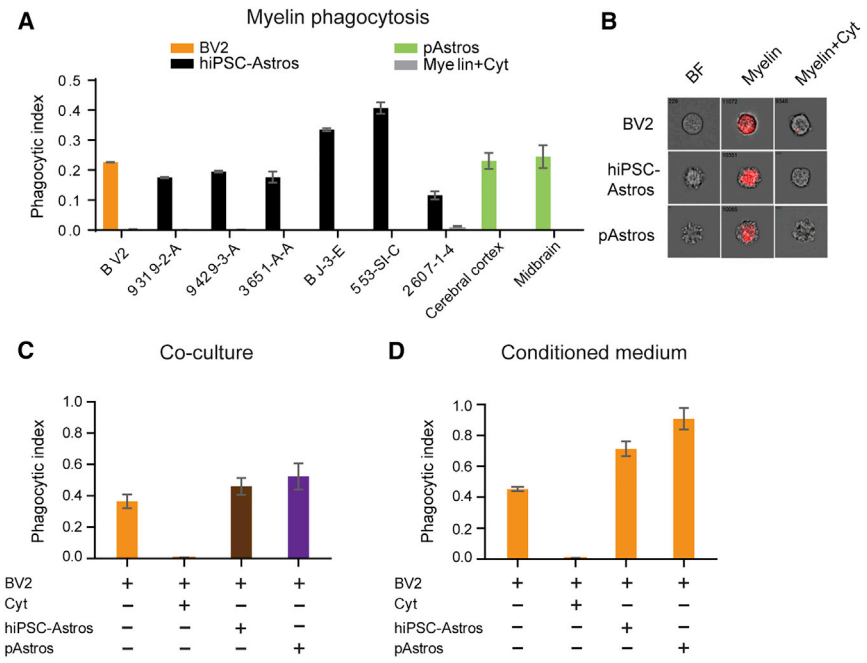

Figure 4. Impact of hiPSC-Astrocytes on the Phagocytic Capacity of BV2 Microglial Cells

(A) Phagocytic indices of BV2 cells, hiPSC-astrocytes, and pAstrocytes incubated with 20 μg of pHrodo-labeled myelin for 3 hr and analyzed by flow cytometry.

(B) Amnis images representative of pHrodo red myelin after engulfment in hiPSC-astrocytes, pAstrocytes, and BV2 cells.

(C) Phagocytic indices of BV2 microglia co-cultured with hiPSC-astrocytes and pAstrocytes that were treated with 30 μg of pHrodo-labeled zymosan for 3 hr and analyzed by flow cytometry, $F(3, 33) = 79.33$.

(D) Phagocytic indices of BV2 microglia treated with astrocyte conditioned medium for 20 hr and then incubated with 30 μg of pHrodo-labeled zymosan for 3 hr for analysis by flow cytometry, $F(3, 13) = 30.80$. Data are representative of three independent experiments from 6–8 different control hiPSC-astrocytes and 2–4 different pAstrocytes and are shown as mean ± SEM. Similar significance was obtained in two other independent experiments. hiPSC-Astros, hiPSC-astrocytes; pAstros, primary human fetal astrocytes. Treatment with 2 μM cytochalasin D (Cyt) was used as a negative control for phagocytosis inhibition.

frequency of spontaneous activity, the number of spontaneous spikes per time, and the amplitude of the calcium spike (Figures 5E–5G). There was no statistical difference in the frequency and number of spikes between hiPSC-astrocytes and primary astrocytes. Interestingly, the amplitude of the spontaneous calcium spike was significantly higher in hiPSC-astrocytes compared with primary astrocytes. Taken together, the excitability of hiPSC-astrocytes was largely indistinguishable from that of primary human astrocytes.

DISCUSSION

We screened 11 methods to differentiate hiPSC-derived NPCs into astrocytes, identifying a medium with low FBS (1%–2%) that produces populations of hiPSC-astrocytes within 30 days. Although this is a commercial medium sold for the culture of primary astrocytes, it has not previously been demonstrated to support differentiation of hiPSC to astrocytes. Our method is fast and robust: unlike previous reports, it does not require prolonged culture (~6 months) or a serial sorting process (Krencik et al., 2011; Shaltouki et al., 2013; Yuan et al., 2011). This protocol was evaluated across 42 NPC lines from 30 individuals (16 males and 14 females) generated from three independent hiPSC cohorts (Table S2). We caution that the quality of the starting NPC population is a critical predictor of success and note that for a few particularly intransient NPC lines, starting from very low-passage stocks proved critical to the ultimate successful differentiation of hiPSC-astrocytes. By both fluorescence-activated cell sorting and qPCR, GFAP seems to be a more variable marker of astrocyte fate (Figures 1A and 1B) and we recommend instead using S100β when evaluating hiPSC-astrocyte populations; moreover, more than any single gene, using panels of markers and/or global transcriptomic analysis more fully reveals the extent of astrocyte patterning of each line. We also suggest that hiPSC-astrocyte response to inflammatory stimuli might represent a simple and easy platform by which to confirm the functionality of hiPSC-astrocytes; astrocytes undergo stimulation-dependent cytokine secretion, while NPCs do not secrete cytokines.

To our knowledge, our method is distinct from others recently reported (Chen et al., 2015; Haidet-Phillips et al., 2014; Jiang et al., 2013; Krencik et al., 2011; McGivern et al., 2013; Serio et al., 2013; Shaltouki et al., 2013), its major advantage being the ease by which hiPSC-astrocytes can be concurrently differentiated from many NPCs from multiple individuals, owing to the simplicity of the protocol, and furthermore that astrocytes can be expanded for months and cryopreserved, serving as a source of cells to support an array of experiments. Therefore, because our protocols for NPC and astrocyte culture are robust and

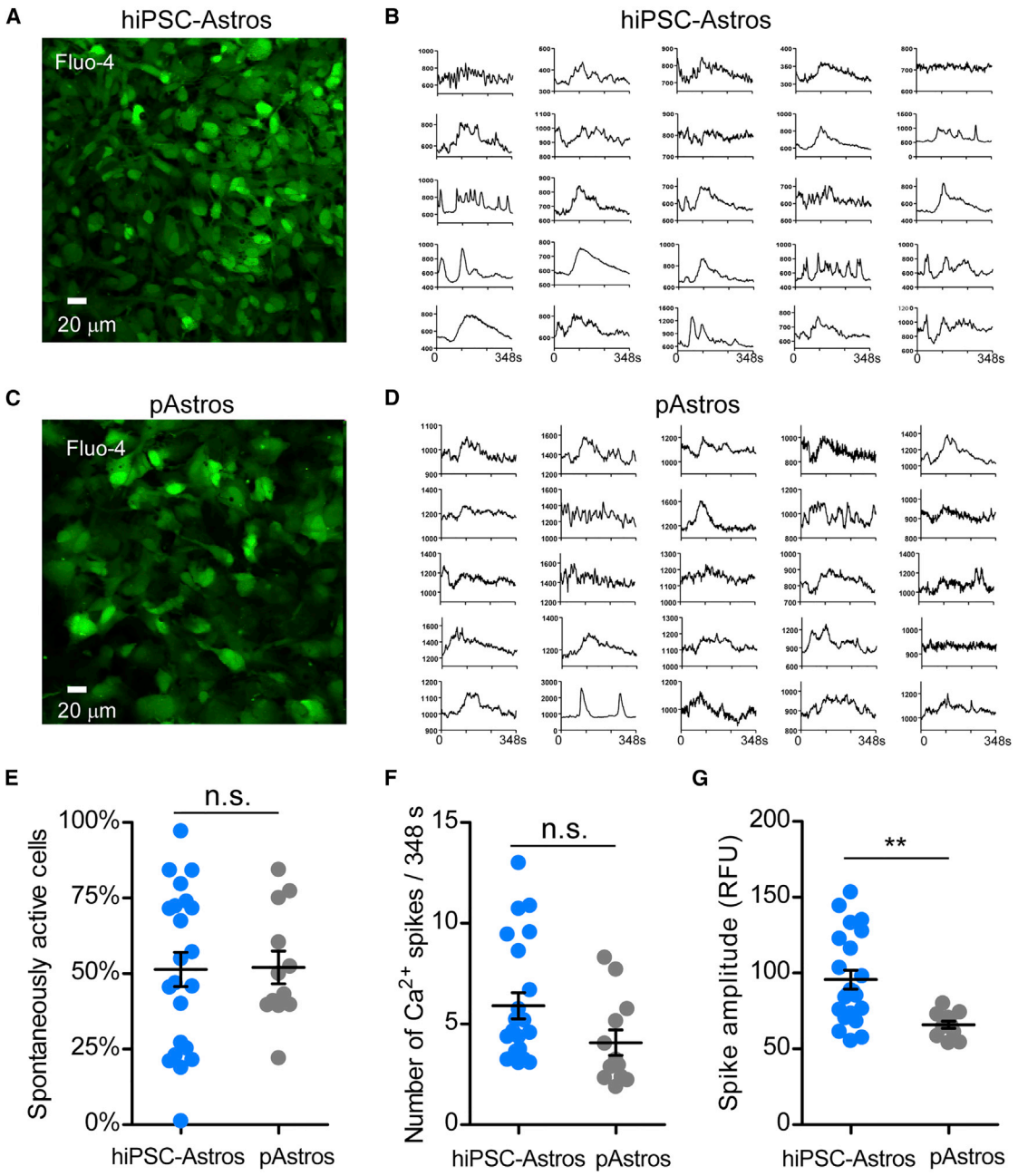

Figure 5. Spontaneous and Glutamate-Responsive Calcium Transients in hiPSC-Astrocytes and Primary Astrocytes

(A and C) Representative Fluo-4-stained hiPSC-astrocytes and pAstrocytes. Note similarity in shape of cells.

(B and D) Plots of fluorescence (RFUs) versus time for 25 regions of interest from hiPSC-astrocytes and pAstrocytes.

(E) Average number of spontaneously active cells per field (318 μm^2) for hiPSC-astrocytes (n = 22 fields from four different lines) and pAstrocytes (n = 12 fields from three different preparations of cerebral cortex astrocytes). n, the number of fields.

(F) Average number of calcium spikes per 348-s trace for hiPSC-astrocytes (n = 22) and pAstrocytes (n = 12).

(G) Average amplitude of calcium spike in each 348-s trace for hiPSC-astrocytes (n = 22) and pAstrocytes (n = 12). Peak excludes the amplitude of the glutamate-induced spike. Each point represents the average multiple regions of interest per 318 μm^2. Line shows mean ± SEM. hiPSC-Astros, hiPSC-astrocytes, pAstros, primary human fetal astrocytes. Using a two-tailed Student's t test, n.s., not significant; **$p < 0.05$.

easily scaled, this methodology is both preferable for large case-control studies from dozens of idiopathic patients and highly amenable to automated culture and future high-throughput drug screens using patient-derived astrocytes (Xu et al., 2016).

We have established a platform for querying astrocyte-specific contributions to disease predisposition in hiPSC-based models. hiPSC-astrocytes closely resemble primary human fetal astrocytes, purified adult brain astrocytes (Zhang et al., 2016), and brain tissue homogenate (Miller et al., 2014) (Figures 2 and 3A). Although the transcriptional profile of our hiPSC-astrocytes most closely resembles a quiescent state (Figure 3B), hiPSC-astrocytes secrete various cytokines and chemokines in response to neuroinflammatory stimuli (Figures 3C and 3D). hiPSC-astrocytes displayed phagocytic capacity (Figure 4A) and enhanced the phagocytic function of microglia in a co-culture assay (Figure 4C). They also showed spontaneous calcium transient activity and responses to glutamate stimulus (Figure 5). Moreover, because nearly pure populations of excitatory neurons and astrocytes from the same individual, hiPSC clone, and even NPC batch can now be compared, our protocol may reduce experimental variation in studies of the cell-autonomous and non-cell-autonomous factors underlying disease predisposition.

While many studies of neurodegeneration and synaptic dysfunction use either primary mouse or human fetal glia for human neuron co-culture (Johnson et al., 2007; Kiskinis et al., 2014; Verheyen et al., 2015), these methods are limited by species-specific differences in astrocyte functions and limited access to human fetal samples. Our hiPSC-astrocytes overcome these drawbacks, making possible hiPSC-based astrocyte-neuron (Jiang et al., 2013) and astrocyte-microglia (Muffat et al., 2016; Pandya et al., 2017) co-culture platforms for uncovering disease-related mechanisms *in vitro*, which should help to reveal how the crosstalk between these three neural cell types contributes to neurological and psychiatric disease.

EXPERIMENTAL PROCEDURES

Human subject work on these de-identified control hiPSCs was approved by the Institutional Review Board at Icahn School of Medicine at Mount Sinai. Control mouse brain tissue was obtained from the Center for Comparative Medicine and Surgery at Icahn School of Medicine at Mount Sinai.

NPCs and Astrocyte Cell Culture

Forebrain NPCs were maintained at high density, grown on Matrigel (BD Bioscience) in NPC medium (DMEM/F12, 1× N2, 1× B27-RA [Invitrogen], 1 mg/mL laminin [Invitrogen], and 20 ng/mL FGF2 [Invitrogen]), and split approximately 1:3 to 1:4 every week with Accutase (Millipore). NPCs could be expanded up to 14 passages. Forebrain NPCs were differentiated to astrocytes by seeding dissociated single cells at 15,000 cells/cm^2 density on Matrigel-coated plates in astrocyte medium (ScienCell: 1801, astrocyte medium [1801-b], 2% fetal bovine serum [0010], astrocyte growth supplement [1852] and 10 U/mL penicillin/streptomycin solution [0503]). Initial NPC quality, seeding density, and single-cell dissociation are critical, particularly during the first 30 days of differentiation, in order to efficiently generate hiPSC-astrocytes. See detailed protocol for astrocyte differentiation from hiPSC-derived NPCs in the Supplemental Information.

Immunocytochemistry

Cultures were washed with PBS and fixed using 4% paraformaldehyde (no. 15714, Electron Microscopy Sciences) for 20 min, then washed three times with PBS 1× plus 0.01% Triton X-100 prior to preincubation with blocking solution made of PBS 1× plus 0.01% Triton X-100 and 10% donkey serum (Sigma-Aldrich), for at least 1 hr. Cultures were then incubated in primary antibody solution overnight at 4°C, followed by an incubation with secondary antibodies for 1 hr at room temperature. See Supplemental Experimental Procedures for antibody details and confocal microscopy.

Real-Time qPCR

The total RNA was extracted from cultured cells with an RNeasy mini kit (no. 74106, Qiagen) and reverse transcribed into cDNA with an iScript cDNA Synthesis kit (no. 1708890, Bio-Rad). cDNA was used as template for the qPCR using a 7900 Real-Time PCR system (Applied Biosystems) with Power SYBR Green PCR Master Mix. The primers used are listed in Table S3. Gene expression was analyzed using the ΔΔCt method. All results were normalized to *GAPDH*, *β-ACTIN*, and *TBP* (TATA-box binding protein) expression, and the values of uninduced fibroblasts were set to 1. Three replicates were used to determine the error bars. See the Supplemental Information for RNA expression studies for qRT-PCR and primer sequences.

Analysis of RNA-Seq Data

Pair-ended RNA-seq data was generated using the Illumina HiSeq 2500 platform for hiPSC-astrocytes (four lines), neurons (six lines), and NPCs (eight lines) (Table S2), as well as for two primary astrocyte samples. The pair-ended sequencing reads were aligned to human hg19 genome using Star Aligner (version 2.5.0b). Following read alignment, featureCounts (Liao et al., 2014) was used to quantify the gene expression at the gene level based on Ensembl gene model GRCh37.70. Gene expression data preprocessing and downstream analyses, including differential gene expression and functional enrichment, are detailed in Supplemental Experimental Procedures.

IL-6 ELISA, Multi-Analyte ELISArray, and Protein Array

hiPSC-astrocytes and primary astrocytes were seeded in astrocyte medium 1 day before the experiment. Cells were treated for 24 hr with 50 ng/mL or 100 ng/mL of poly(I:C) (InvivoGen, no. tlrl-pic), 10 μg/mL or 50 μg/mL of LPS (Sigma-Aldrich, no.

L5886), and 5 μM or 10 μM human β-amyloid (Aβ42) (California-Peptide, no. 641-15) and vehicle control solutions (saline for poly(I:C) and LPS or Tris-HCl for Aβ42). Samples were analyzed with IL-6 ELISA assay (Affymetrix eBioscience, no. 88-7066), Human Inflammatory Cytokines Multi-Analyte ELISArray (Qiagen, no. MEH-004A), RT2 Profiler PCR Arrays (Qiagen), and Proteome Profiler Human Cytokine Array (R&D Systems, no. ARY005B). For a detailed protocol see Supplemental Experimental Procedures.

Phagocytosis Assay

Phagocytic capacity of hiPSC-astrocytes, primary astrocytes, and BV2 cells was analyzed by incubating cells with pHrodo-labeled zymosan (Thermo Fisher, P35364) or myelin purified from mouse brains, and then measured by flow cytometry. Detailed protocols for co-culture experiments and astrocyte conditioned media treatment are provided in the Supplemental Experimental Procedures.

Calcium Imaging

Cells were incubated with 2 μM Fluo-4AM (Molecular Probes) and 0.02% Pluronic F 127 detergent in Krebs HEPES buffer (KHB). Time-lapse image sequences (×40 magnification) were acquired at 0.9 Hz and analyzed by FluoroSNNAP software operated by MATLAB. For a detailed protocol see Supplemental Experimental Procedures.

Statistical Analysis

For all experiments, data are represented as mean ± SD or SEM of three to five biological replicates. Statistical significance was determined using a two-tailed homoscedastic Student's t test or one-way ANOVA and Tukey-Kramer post hoc test for differences of means between each group of data with parametric distribution. Significant comparisons are labeled in the figures as *$p < 0.05$, **$p < 0.01$, and ***$p < 0.001$.

Extended experimental procedures and any associated references are available in the online version of this paper.

ACCESSION NUMBERS

The accession number for the RNA-seq data reported in this paper is GEO: GSE97904.

SUPPLEMENTAL INFORMATION

Supplemental Information includes Supplemental Experimental Procedures, four figures, and five tables and can be found with this article online at http://dx.doi.org/10.1016/j.stemcr.2017.06.018.

AUTHOR CONTRIBUTIONS

J.TCW, K.J.B., and A.M.G. designed the experiments and wrote the manuscript. J.TCW developed the astrocyte differentiation protocol. J.TCW, K.R.B., B.J.H., and R.A. (with H.P.) differentiated the hiPSC-astrocyte lines. M.W. and B.Z. conducted the RNA-seq analysis. J.TCW performed the neuroinflammatory assays. A.A.P., J.TCW, and S.I.M. performed the phagocytosis assays. J.TCW, A.A.P., and B.J.H. executed flow-cytometry analysis on astrocytes and NPCs. J.TCW and K.R.B. performed real-time qPCR and immunofluorescence staining. E.L. and P.A.S. conducted and analyzed the calcium imaging analysis. C.M.K. shared prepublication information about astrocyte differentiation conditions.

ACKNOWLEDGMENTS

BV2 cell line was kindly provided by Marc Diamond (UT Southwestern Medical Center). We are grateful for the continuous support of the Flow Cytometry Core at the Icahn School of Medicine at Mount Sinai Hospital. This work was supported in part by the JPB Foundation (A.M.G.), the Rainwater Foundation (A.M.G.), NIMH R01MH101454 (K.J.B.), NIA U01P50AG005138-30-1 (Alzheimer's Disease Research Center: Pilot 30-1) (K.J.B.), NIA/NIH U01AG046170 (K.J.B., M.W., and B.Z.), a component of the AMP-AD Target Discovery and Preclinical Validation Project, NIMH R01MH11499 (P.A.S.), NIAAA R01AA018734 (P.A.S.), NIDA R01DA037170 (P.A.S.), K01AG046374 (C.M.K.), and the New York Stem Cell Foundation (K.J.B.) and Project ALS (H.P.). A.M.G. serves on the Scientific Advisory Board for Denali Therapeutics.

Received: April 30, 2017
Revised: June 28, 2017
Accepted: June 29, 2017
Published: July 27, 2017

REFERENCES

Ballas, N., Lioy, D.T., Grunseich, C., and Mandel, G. (2009). Non-cell autonomous influence of MeCP2-deficient glia on neuronal dendritic morphology. Nat. Neurosci. *12*, 311–317.

Barres, B.A. (2008). The mystery and magic of glia: a perspective on their roles in health and disease. Neuron *60*, 430–440.

Bi, F., Huang, C., Tong, J., Qiu, G., Huang, B., Wu, Q., Li, F., Xu, Z., Bowser, R., Xia, X.G., et al. (2013). Reactive astrocytes secrete lcn2 to promote neuron death. Proc. Natl. Acad. Sci. USA *110*, 4069–4074.

Boyles, J.K., Pitas, R.E., Wilson, E., Mahley, R.W., and Taylor, J.M. (1985). Apolipoprotein E associated with astrocytic glia of the central nervous system and with nonmyelinating glia of the peripheral nervous system. J. Clin. Invest. *76*, 1501–1513.

Bradford, J., Shin, J.Y., Roberts, M., Wang, C.E., Li, X.J., and Li, S. (2009). Expression of mutant huntingtin in mouse brain astrocytes causes age-dependent neurological symptoms. Proc. Natl. Acad. Sci. USA *106*, 22480–22485.

Brennand, K.J., and Gage, F.H. (2011). Concise review: the promise of human induced pluripotent stem cell-based studies of schizophrenia. Stem Cells *29*, 1915–1922.

Brennand, K., Savas, J.N., Kim, Y., Tran, N., Simone, A., Hashimoto-Torii, K., Beaumont, K.G., Kim, H.J., Topol, A., Ladran, I., et al. (2015). Phenotypic differences in hiPSC NPCs derived from patients with schizophrenia. Mol. Psychiatry *20*, 361–368.

Cahoy, J.D., Emery, B., Kaushal, A., Foo, L.C., Zamanian, J.L., Christopherson, K.S., Xing, Y., Lubischer, J.L., Krieg, P.A., Krupenko, S.A., et al. (2008). A transcriptome database for astrocytes, neurons, and oligodendrocytes: a new resource for understanding brain development and function. J. Neurosci. *28*, 264–278.

Chaboub, L.S., and Deneen, B. (2013). Astrocyte form and function in the developing central nervous system. Semin. Pediatr. Neurol. *20*, 230–235.

Chen, H., Qian, K., Chen, W., Hu, B., Blackbourn, L.W., Du, Z., Ma, L., Liu, H., Knobel, K.M., Ayala, M., et al. (2015). Human-derived neural progenitors functionally replace astrocytes in adult mice. J. Clin. Invest. *125*, 1033–1042.

Chung, W.S., Clarke, L.E., Wang, G.X., Stafford, B.K., Sher, A., Chakraborty, C., Joung, J., Foo, L.C., Thompson, A., Chen, C., et al. (2013). Astrocytes mediate synapse elimination through MEGF10 and MERTK pathways. Nature *504*, 394–400.

Di Giorgio, F.P., Boulting, G.L., Bobrowicz, S., and Eggan, K.C. (2008). Human embryonic stem cell-derived motor neurons are sensitive to the toxic effect of glial cells carrying an ALS-causing mutation. Cell Stem Cell *3*, 637–648.

Eroglu, C., and Barres, B.A. (2010). Regulation of synaptic connectivity by glia. Nature *468*, 223–231.

Freeman, M.R., and Rowitch, D.H. (2013). Evolving concepts of gliogenesis: a look way back and ahead to the next 25 years. Neuron *80*, 613–623.

Garwood, C.J., Pooler, A.M., Atherton, J., Hanger, D.P., and Noble, W. (2011). Astrocytes are important mediators of Abeta-induced neurotoxicity and tau phosphorylation in primary culture. Cell Death Dis. *2*, e167.

Haidet-Phillips, A.M., Roybon, L., Gross, S.K., Tuteja, A., Donnelly, C.J., Richard, J.P., Ko, M., Sherman, A., Eggan, K., Henderson, C.E., et al. (2014). Gene profiling of human induced pluripotent stem cell-derived astrocyte progenitors following spinal cord engraftment. Stem Cells Transl. Med. *3*, 575–585.

Han, X., Chen, M., Wang, F., Windrem, M., Wang, S., Shanz, S., Xu, Q., Oberheim, N.A., Bekar, L., Betstadt, S., et al. (2013). Forebrain engraftment by human glial progenitor cells enhances synaptic plasticity and learning in adult mice. Cell Stem Cell *12*, 342–353.

Heni, M., Hennige, A.M., Peter, A., Siegel-Axel, D., Ordelheide, A.M., Krebs, N., Machicao, F., Fritsche, A., Haring, H.U., and Staiger, H. (2011). Insulin promotes glycogen storage and cell proliferation in primary human astrocytes. PLoS One *6*, e21594.

Hubbard, J.A., Hsu, M.S., Seldin, M.M., and Binder, D.K. (2015). Expression of the astrocyte water channel aquaporin-4 in the mouse brain. ASN Neuro *7*. http://dx.doi.org/10.1177/1759091415605486.

Jana, M., Palencia, C.A., and Pahan, K. (2008). Fibrillar amyloid-beta peptides activate microglia via TLR2: implications for Alzheimer's disease. J. Immunol. *181*, 7254–7262.

Jiang, P., Chen, C., Wang, R., Chechneva, O.V., Chung, S.H., Rao, M.S., Pleasure, D.E., Liu, Y., Zhang, Q., and Deng, W. (2013). hESC-derived Olig2+ progenitors generate a subtype of astroglia with protective effects against ischaemic brain injury. Nat. Commun. *4*, 2196.

Johnson, M.A., Weick, J.P., Pearce, R.A., and Zhang, S.C. (2007). Functional neural development from human embryonic stem cells: accelerated synaptic activity via astrocyte coculture. J. Neurosci. *27*, 3069–3077.

Kiskinis, E., Sandoe, J., Williams, L.A., Boulting, G.L., Moccia, R., Wainger, B.J., Han, S., Peng, T., Thams, S., Mikkilineni, S., et al. (2014). Pathways disrupted in human ALS motor neurons identified through genetic correction of mutant SOD1. Cell Stem Cell *14*, 781–795.

Krencik, R., Weick, J.P., Liu, Y., Zhang, Z.J., and Zhang, S.C. (2011). Specification of transplantable astroglial subtypes from human pluripotent stem cells. Nat. Biotechnol. *29*, 528–534.

Lee, C.Y., and Landreth, G.E. (2010). The role of microglia in amyloid clearance from the AD brain. J. Neural Transm. (Vienna) *117*, 949–960.

Liao, Y., Smyth, G.K., and Shi, W. (2014). featureCounts: an efficient general purpose program for assigning sequence reads to genomic features. Bioinformatics *30*, 923–930.

Ludwin, S.K., Kosek, J.C., and Eng, L.F. (1976). The topographical distribution of S-100 and GFA proteins in the adult rat brain: an immunohistochemical study using horseradish peroxidase-labelled antibodies. J. Comp. Neurol. *165*, 197–207.

Marchetto, M.C., Muotri, A.R., Mu, Y., Smith, A.M., Cezar, G.G., and Gage, F.H. (2008). Non-cell-autonomous effect of human SOD1 G37R astrocytes on motor neurons derived from human embryonic stem cells. Cell Stem Cell *3*, 649–657.

Marinelli, C., Di Liddo, R., Facci, L., Bertalot, T., Conconi, M.T., Zusso, M., Skaper, S.D., and Giusti, P. (2015). Ligand engagement of Toll-like receptors regulates their expression in cortical microglia and astrocytes. J. Neuroinflammation *12*, 244.

McGivern, J.V., Patitucci, T.N., Nord, J.A., Barabas, M.E., Stucky, C.L., and Ebert, A.D. (2013). Spinal muscular atrophy astrocytes exhibit abnormal calcium regulation and reduced growth factor production. Glia *61*, 1418–1428.

Mertens, J., Marchetto, M.C., Bardy, C., and Gage, F.H. (2016). Evaluating cell reprogramming, differentiation and conversion technologies in neuroscience. Nat. Rev. Neurosci. *17*, 424–437.

Miller, J.A., Ding, S.L., Sunkin, S.M., Smith, K.A., Ng, L., Szafer, A., Ebbert, A., Riley, Z.L., Royall, J.J., Aiona, K., et al. (2014). Transcriptional landscape of the prenatal human brain. Nature *508*, 199–206.

Muffat, J., Li, Y., Yuan, B., Mitalipova, M., Omer, A., Corcoran, S., Bakiasi, G., Tsai, L.H., Aubourg, P., Ransohoff, R.M., et al. (2016). Efficient derivation of microglia-like cells from human pluripotent stem cells. Nat. Med. *22*, 1358–1367.

Oberheim, N.A., Takano, T., Han, X., He, W., Lin, J.H., Wang, F., Xu, Q., Wyatt, J.D., Pilcher, W., Ojemann, J.G., et al. (2009). Uniquely hominid features of adult human astrocytes. J. Neurosci. *29*, 3276–3287.

Palm, T., Bolognin, S., Meiser, J., Nickels, S., Trager, C., Meilenbrock, R.L., Brockhaus, J., Schreitmuller, M., Missler, M., and Schwamborn, J.C. (2015). Rapid and robust generation of long-term self-renewing human neural stem cells with the ability to generate mature astroglia. Sci. Rep. *5*, 16321.

Pandya, H., Shen, M.J., Ichikawa, D.M., Sedlock, A.B., Choi, Y., Johnson, K.R., Kim, G., Brown, M.A., Elkahloun, A.G., Maric, D., et al. (2017). Differentiation of human and murine induced pluripotent stem cells to microglia-like cells. Nat. Neurosci. *20*, 753–759.

Papadeas, S.T., Kraig, S.E., O'Banion, C., Lepore, A.C., and Maragakis, N.J. (2011). Astrocytes carrying the superoxide dismutase 1 (SOD1G93A) mutation induce wild-type motor neuron degeneration in vivo. Proc. Natl. Acad. Sci. USA *108*, 17803–17808.

Pinkas-Kramarski, R., Eilam, R., Spiegler, O., Lavi, S., Liu, N., Chang, D., Wen, D., Schwartz, M., and Yarden, Y. (1994). Brain neurons and glial cells express Neu differentiation factor/heregulin: a survival factor for astrocytes. Proc. Natl. Acad. Sci. USA *91*, 9387–9391.

Richard, K.L., Filali, M., Prefontaine, P., and Rivest, S. (2008). Toll-like receptor 2 acts as a natural innate immune receptor to clear amyloid beta 1-42 and delay the cognitive decline in a mouse model of Alzheimer's disease. J. Neurosci. *28*, 5784–5793.

Rothstein, J.D., Martin, L., Levey, A.I., Dykes-Hoberg, M., Jin, L., Wu, D., Nash, N., and Kuncl, R.W. (1994). Localization of neuronal and glial glutamate transporters. Neuron *13*, 713–725.

Roybon, L., Lamas, N.J., Garcia-Diaz, A., Yang, E.J., Sattler, R., Jackson-Lewis, V., Kim, Y.A., Kachel, C.A., Rothstein, J.D., Przedborski, S., et al. (2013). Human stem cell-derived spinal cord astrocytes with defined mature or reactive phenotypes. Cell Rep. *4*, 1035–1048.

Scemes, E., and Giaume, C. (2006). Astrocyte calcium waves: what they are and what they do. Glia *54*, 716–725.

Schnitzer, J., Franke, W.W., and Schachner, M. (1981). Immunocytochemical demonstration of vimentin in astrocytes and ependymal cells of developing and adult mouse nervous system. J. Cell Biol. *90*, 435–447.

Seifert, G., Schilling, K., and Steinhauser, C. (2006). Astrocyte dysfunction in neurological disorders: a molecular perspective. Nat. Rev. Neurosci. *7*, 194–206.

Serio, A., Bilican, B., Barmada, S.J., Ando, D.M., Zhao, C., Siller, R., Burr, K., Haghi, G., Story, D., Nishimura, A.L., et al. (2013). Astrocyte pathology and the absence of non-cell autonomy in an induced pluripotent stem cell model of TDP-43 proteinopathy. Proc. Natl. Acad. Sci. USA *110*, 4697–4702.

Shaltouki, A., Peng, J., Liu, Q., Rao, M.S., and Zeng, X. (2013). Efficient generation of astrocytes from human pluripotent stem cells in defined conditions. Stem Cells *31*, 941–952.

Sherwood, C.C., Stimpson, C.D., Raghanti, M.A., Wildman, D.E., Uddin, M., Grossman, L.I., Goodman, M., Redmond, J.C., Bonar, C.J., Erwin, J.M., et al. (2006). Evolution of increased glia-neuron ratios in the human frontal cortex. Proc. Natl. Acad. Sci. USA *103*, 13606–13611.

Skripuletz, T., Hackstette, D., Bauer, K., Gudi, V., Pul, R., Voss, E., Berger, K., Kipp, M., Baumgartner, W., and Stangel, M. (2013). Astrocytes regulate myelin clearance through recruitment of microglia during cuprizone-induced demyelination. Brain *136*, 147–167.

Tong, X., Ao, Y., Faas, G.C., Nwaobi, S.E., Xu, J., Haustein, M.D., Anderson, M.A., Mody, I., Olsen, M.L., Sofroniew, M.V., et al. (2014). Astrocyte Kir4.1 ion channel deficits contribute to neuronal dysfunction in Huntington's disease model mice. Nat. Neurosci. *17*, 694–703.

Verheyen, A., Diels, A., Dijkmans, J., Oyelami, T., Meneghello, G., Mertens, L., Versweyveld, S., Borgers, M., Buist, A., Peeters, P., et al. (2015). Using human iPSC-derived neurons to model TAU aggregation. PLoS One *10*, e0146127.

Volterra, A., Liaudet, N., and Savtchouk, I. (2014). Astrocyte Ca(2)(+) signalling: an unexpected complexity. Nat. Rev. Neurosci. *15*, 327–335.

Wyss-Coray, T., Loike, J.D., Brionne, T.C., Lu, E., Anankov, R., Yan, F., Silverstein, S.C., and Husemann, J. (2003). Adult mouse astrocytes degrade amyloid-beta in vitro and in situ. Nat. Med. *9*, 453–457.

Xu, Q., Bernardo, A., Walker, D., Kanegawa, T., Mahley, R.W., and Huang, Y. (2006). Profile and regulation of apolipoprotein E (ApoE) expression in the CNS in mice with targeting of green fluorescent protein gene to the ApoE locus. J. Neurosci. *26*, 4985–4994.

Xu, M., Lee, E.M., Wen, Z., Cheng, Y., Huang, W.K., Qian, X., Tcw, J., Kouznetsova, J., Ogden, S.C., Hammack, C., et al. (2016). Identification of small-molecule inhibitors of Zika virus infection and induced neural cell death via a drug repurposing screen. Nat. Med. *22*, 1101–1107.

Yuan, S.H., Martin, J., Elia, J., Flippin, J., Paramban, R.I., Hefferan, M.P., Vidal, J.G., Mu, Y., Killian, R.L., Israel, M.A., et al. (2011). Cell-surface marker signatures for the isolation of neural stem cells, glia and neurons derived from human pluripotent stem cells. PLoS One *6*, e17540.

Zamanian, J.L., Xu, L., Foo, L.C., Nouri, N., Zhou, L., Giffard, R.G., and Barres, B.A. (2012). Genomic analysis of reactive astrogliosis. J. Neurosci. *32*, 6391–6410.

Zhang, Y., and Barres, B.A. (2010). Astrocyte heterogeneity: an underappreciated topic in neurobiology. Curr. Opin. Neurobiol. *20*, 588–594.

Zhang, Y., Sloan, S.A., Clarke, L.E., Caneda, C., Plaza, C.A., Blumenthal, P.D., Vogel, H., Steinberg, G.K., Edwards, M.S., Li, G., et al. (2016). Purification and characterization of progenitor and mature human astrocytes reveals transcriptional and functional differences with mouse. Neuron *89*, 37–53.

Zhao, B., and Schwartz, J.P. (1998). Involvement of cytokines in normal CNS development and neurological diseases: recent progress and perspectives. J. Neurosci. Res. *52*, 7–16.

Stem Cell Reports, Volume *9*

Supplemental Information

An Efficient Platform for Astrocyte Differentiation from Human Induced Pluripotent Stem Cells

Julia TCW, Minghui Wang, Anna A. Pimenova, Kathryn R. Bowles, Brigham J. Hartley, Emre Lacin, Saima I. Machlovi, Rawan Abdelaal, Celeste M. Karch, Hemali Phatnani, Paul A. Slesinger, Bin Zhang, Alison M. Goate, and Kristen J. Brennand

SUPPLEMENTARY INFORMATION

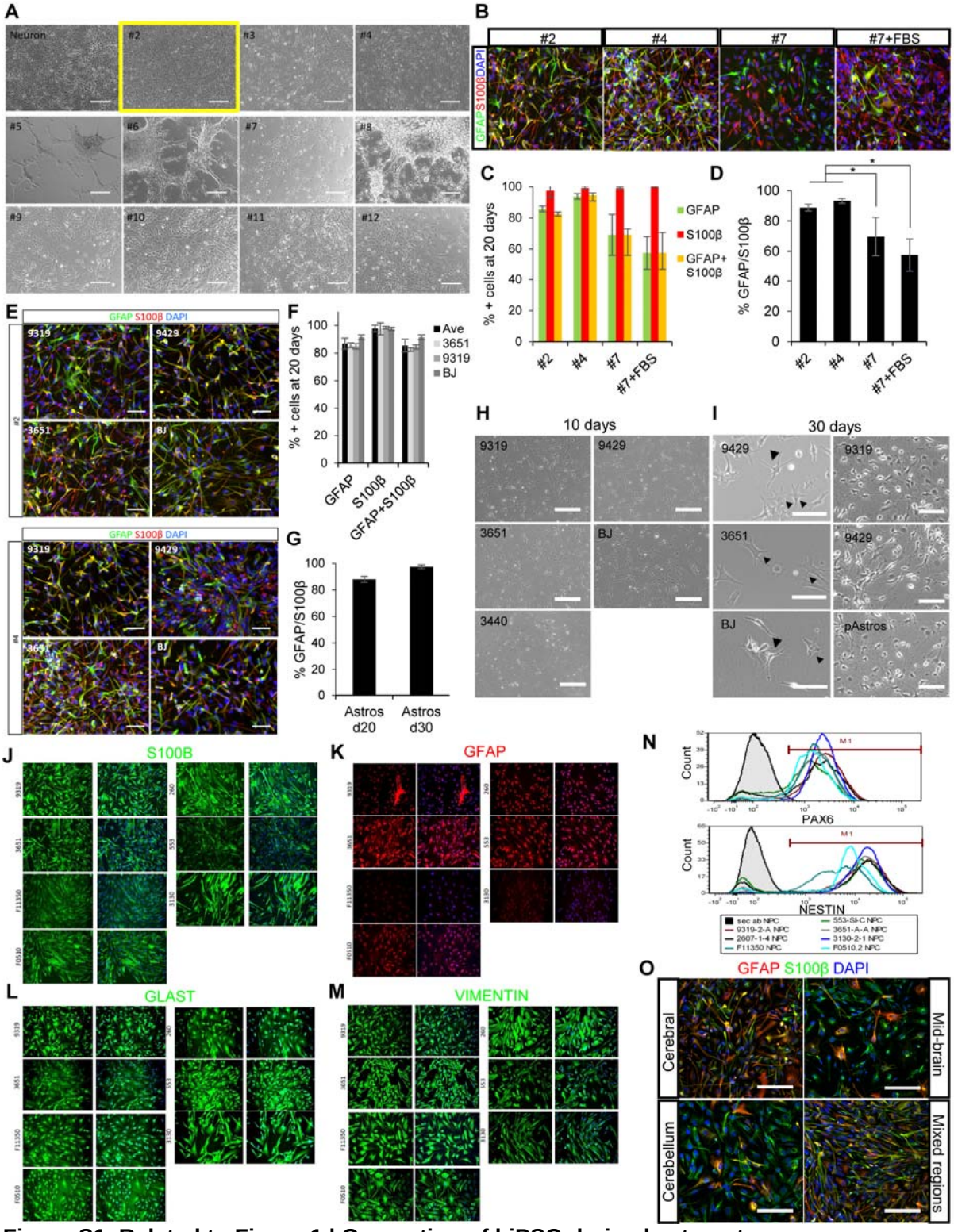

Figure S1. Related to Figure 1 | Generation of hiPSC-derived astrocytes.

(**A**) Cell morphologies across 12 screening conditions including 11 astrocyte differentiation condition and 1 cortical neuron differentiation condition after 20 days of differentiation from

NPCs. (**B**) Representative images of GFAP (green) and S100β (red) positive cells from two cell lines in top four selected conditions from (**A**). (**C**) Quantification of the number of cells positive for GFAP and S100β protein (N=5 from two cell lines) in top four selected conditions from (**A**). (**D**) Quantification of GFAP-positive cells normalized by S100β-positive cells (N=5 from two cell lines in top four selected conditions from (**A**). (**E**) Representative immunofluorescence images of GFAP (green) and S100β (red) across hiPSC-astrocytes differentiated from four control NPC lines (**Table S2**) at 20 days of differentiation using medium #2 condition. Images are quantified in (**F**) and (**G**). (**F**) Quantification of the number of cells positive for GFAP and S100β across hiPSC-astrocytes differentiated from four control NPC lines at 20 days of differentiation using medium #2 condition. (**G**) Percentage of GFAP-positive cells normalized by S100β-positive cells at 20 days and 30 days of differentiation using medium #2 condition. (**H**) Bright field images of hiPSC-astrocytes differentiated from 5 control NPC lines (**Table S2**) showing a similar astrocyte morphology at 10 days after medium #2 exposure. Scale bar = 500 µm. (**I**) Bright field images of hiPSC-astrocytes differentiated from 5 control NPC lines (**Table S2**) at 30 days of differentiation. Arrows represent fibrous-like morphology and arrowheads represent protoplasmic-like morphology of astrocytes. Each cell line includes both shapes of astrocytes (left, Scale bar = 200 µm). Higher density culture displays star-shaped astrocyte morphology (right, Scale bar = 500 µm). (**J-M**) Representative immunofluorescence images of S100β (green), GFAP (red), GLAST (EAAT1) (green) and VIMENTIN (green) of hiPSC-astrocytes differentiated from 7 control NPC lines from three independent hiPSC cohorts (**Table S2**). Scale bar = 200 µm. (**N**) Flow cytometric analysis of PAX6 and NESTIN-positive cells from the 7 isogenic NPC lines used for hiPSC-astrocyte differentiations in **J-M**. M1 represents positive cells expressing each marker protein. (**O**) GFAP (red) and S100β (green)-staining in primary astrocytes from different regions of human fetal brain including cerebral cortex, mid-brain, cerebellum and the whole brain (labeled mixed regions). Scale bar = 200 µm. Data are represented as mean ± error bar (Standard Deviation). hiPSC-Astros: human hiPSC-derived astrocytes, pAstros: primary human fetal astrocytes. A two-tailed homoscedastic Student's t-test, n.s.: not significant, * $p < 0.05$, ** $p < 0.01$, *** $p < 0.001$.

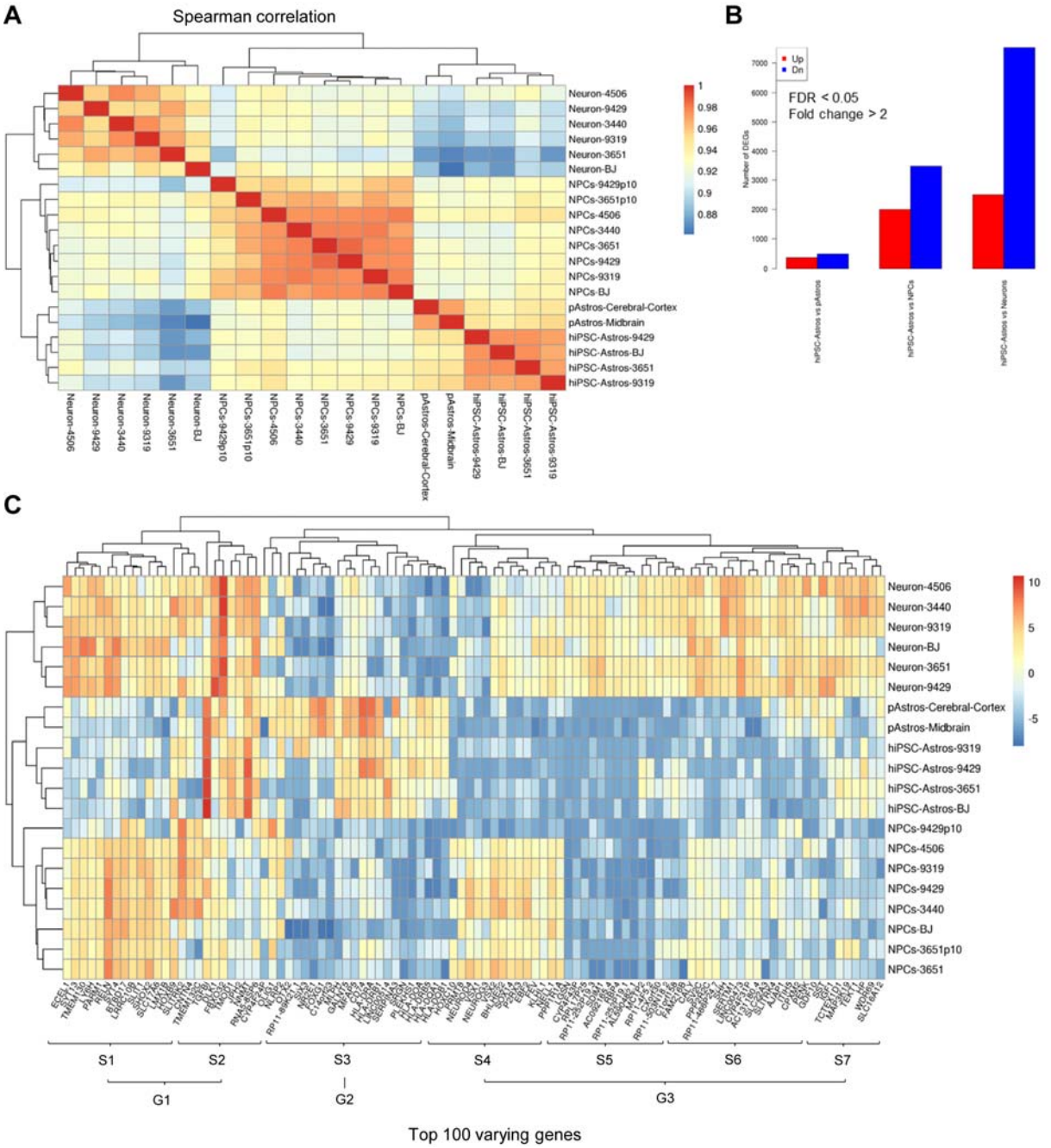

Figure S2. Related to Figure 2 | Global gene expression profiling to compare the transcriptional profile of hiPSC-derived astrocytes and primary human fetal astrocytes.
RNAseq analysis of hiPSC-derived NPCs (N=8), neurons (N=6) and astrocytes (N=4) together with pAstrocytes (N=2) from the cerebral cortex and midbrain region. (**A**) Spearman correlation analysis of hiPSC-derived NPCs, neurons and astrocytes, together with pAstrocytes. (**B**) The number of genes differentially expressed between hiPSC-astrocytes and pAstrocytes, as well as between hiPSC-astrocytes and hiPSC-derived NPCs or neurons: less than 400 genes were differentially expressed (upregulated or downregulated, respectively) in hiPSC-astrocytes relative to pAstrocytes, while nearly 10,000 genes were differentially expressed between hiPSC-astrocytes and hiPSC-neurons. hiPSC-Astros: hiPSC-astrocytes, pAstros: primary astrocytes.

(**C**) Heatmap of hiPSC-derived NPCs, neurons and astrocytes compared to fetal and adult brain tissue (GSE73721) (Zhang et al., 2016) using the top 100 most varying genes, clustered by group (G) 1-3 and sub-group (S) 1-7.

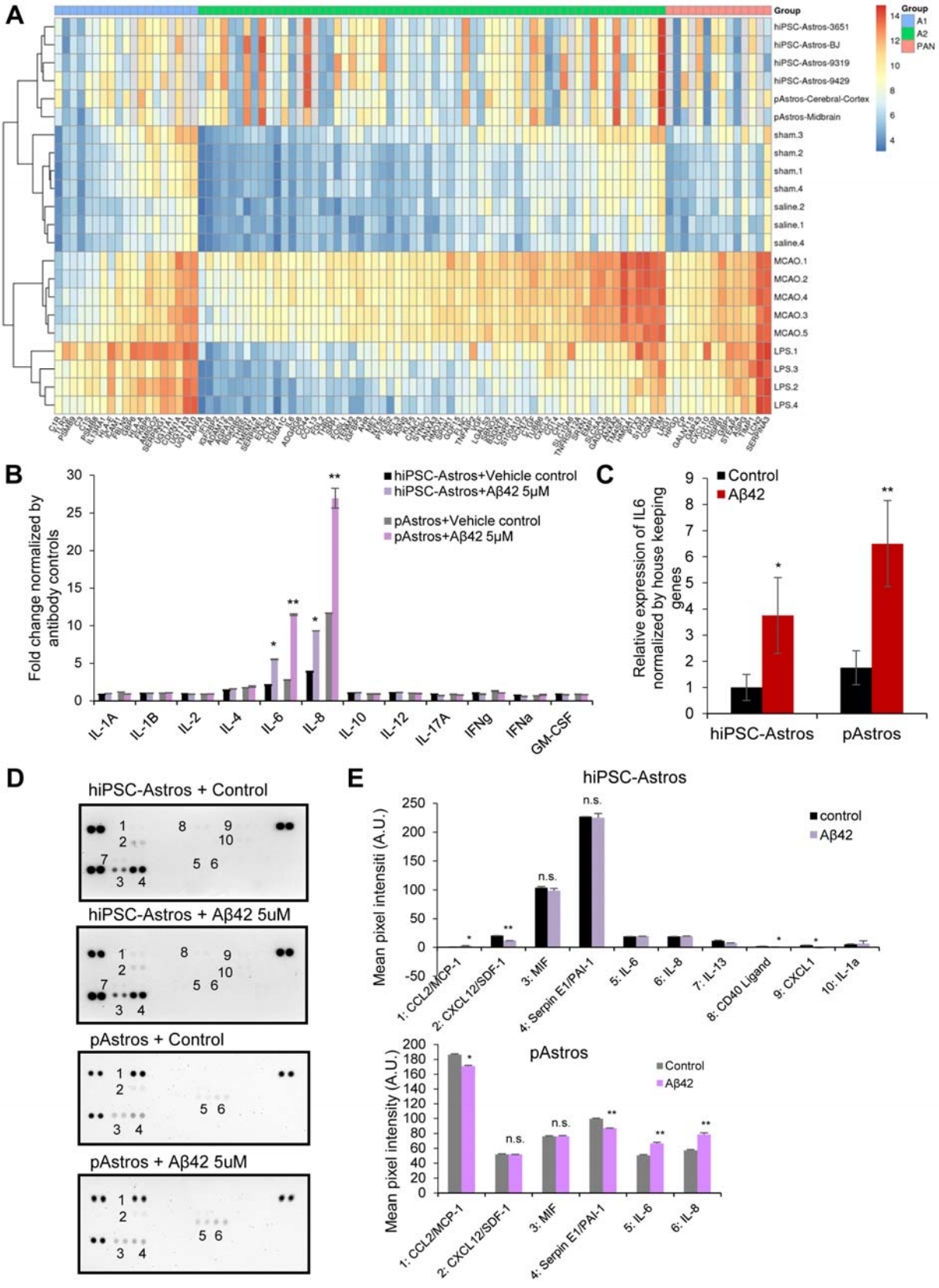
A
Group
hiPSC-Astros-3651
hiPSC-Astros-BJ
hiPSC-Astros-9319
hiPSC-Astros-9429
pAstros-Cerebral-Cortex
pAstros-Midbrain
sham.3
sham.2
sham.1
sham.4
saline.2
saline.1
saline.4
MCAO.1
MCAO.2
MCAO.4
MCAO.3
MCAO.5
LPS.1
LPS.3
LPS.2
LPS.4
Group
A1
A2
PAN
14
12
10
8
6
4
B
Fold change normalized by antibody controls
hiPSC-Astros+Vehicle control
hiPSC-Astros+Aβ42 5μM
pAstros+Vehicle control
pAstros+Aβ42 5μM
IL-1A
IL-1B
IL-2
IL-4
IL-6
IL-8
IL-10
IL-12
IL-17A
IFNg
IFNa
GM-CSF
C
Relative expression of IL6 normalized by house keeping genes
Control
Aβ42
hiPSC-Astros
pAstros
D
hiPSC-Astros + Control
hiPSC-Astros + Aβ42 5uM
pAstros + Control
pAstros + Aβ42 5uM
E
hiPSC-Astros
Mean pixel intensiti (A.U.)
control
Aβ42
1: CCL2/MCP-1
2: CXCL12/SDF-1
3: MIF
4: Serpin E1/PAI-1
5: IL-6
6: IL-8
7: IL-13
8: CD40 Ligand
9: CXCL1
10: IL-1a
pAstros
Mean pixel intensity (A.U.)
Control
Aβ42

Figure S3. Related to Figure 3 | Characterization of the neuroinflammatory status and reactivity of hiPSC-astrocytes.

(**A**) Heatmap-based cluster analysis of hiPSC-astrocytes and pAstrocytes compared to the astrocyte reactivity dataset (Zamanian et al., 2012), which was sorted by reactivity genes enriched in the A1 (LPS-treatment), A2 (MCAO ischemia) and pan-reactive phenotypes, or related controls (saline and sham, respectively). (**B**) Cytokine secretion from hiPSC-astrocytes and pAstrocytes measured by ELISA in response to 24-hour treatment with 5 μM Aβ42. (N=2 from two different hiPSC-astrocyte lines and two independent preparations of pAstrocytes cerebral cortex, N, independent experiments.) (**C**) *IL-6* gene expression changes in samples used for (**D**). (N=3 from two different hiPSC-astrocyte lines and two independent preparations of pAstrocytes cerebral cortex, N, independent experiments.) (**D**) Proteome profiler human cytokine array (targets are listed in **Table S4**) of hiPSC-astrocytes and pAstrocytes, with or without 5 μM Aβ42 treatment. Unlabeled dot blots are positive experimental controls from the manufacturer. (**E**) Quantification of dot blots in (**D**). (N=2 from two different hiPSC-astrocyte lines and two independent preparations of pAstrocytes cerebral cortex, N, independent experiments.) Proteome profiler human cytokine array tests chemokine levels. Data are represented as mean ± SD. hiPSC-Astros: hiPSC-derived astrocytes, pAstros: primary astrocytes. A two-tailed homoscedastic Student's t-test, n.s.: not significant, * $p < 0.05$, ** $p < 0.01$, *** $p < 0.001$

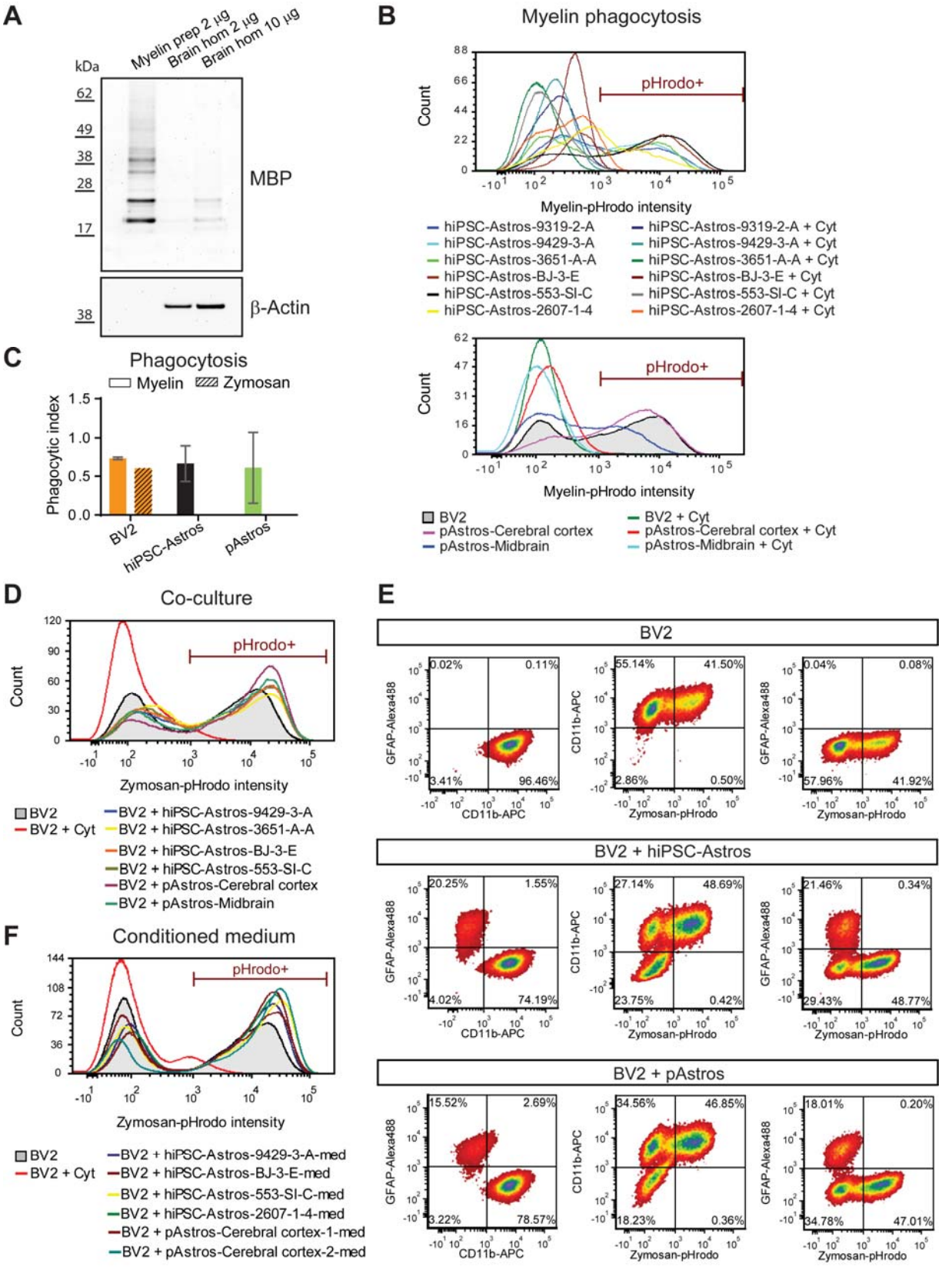
A
Myelin prep 2 µg
Brain hom 2 µg
Brain hom 10 µg
kDa
62
49
38
28
17
MBP
38
β-Actin
B
Myelin phagocytosis
Count
pHrodo+
Myelin-pHrodo intensity
hiPSC-Astros-9319-2-A
hiPSC-Astros-9429-3-A
hiPSC-Astros-3651-A-A
hiPSC-Astros-BJ-3-E
hiPSC-Astros-553-SI-C
hiPSC-Astros-2607-1-4
hiPSC-Astros-9319-2-A + Cyt
hiPSC-Astros-9429-3-A + Cyt
hiPSC-Astros-3651-A-A + Cyt
hiPSC-Astros-BJ-3-E + Cyt
hiPSC-Astros-553-SI-C + Cyt
hiPSC-Astros-2607-1-4 + Cyt
BV2
pAstros-Cerebral cortex
pAstros-Midbrain
BV2 + Cyt
pAstros-Cerebral cortex + Cyt
pAstros-Midbrain + Cyt
C
Phagocytosis
Myelin
Zymosan
Phagocytic index
BV2
hiPSC-Astros
pAstros
D
Co-culture
Zymosan-pHrodo intensity
BV2
BV2 + Cyt
BV2 + hiPSC-Astros-9429-3-A
BV2 + hiPSC-Astros-3651-A-A
BV2 + hiPSC-Astros-BJ-3-E
BV2 + hiPSC-Astros-553-SI-C
BV2 + pAstros-Cerebral cortex
BV2 + pAstros-Midbrain
E
BV2
BV2 + hiPSC-Astros
BV2 + pAstros
GFAP-Alexa488
CD11b-APC
Zymosan-pHrodo
0.02%
0.11%
3.41%
96.46%
55.14%
41.50%
2.86%
0.50%
0.04%
0.08%
57.96%
41.92%
20.25%
1.55%
4.02%
74.19%
27.14%
48.69%
23.75%
0.42%
21.46%
0.34%
29.43%
48.77%
15.52%
2.69%
3.22%
78.57%
34.56%
46.85%
18.23%
0.36%
18.01%
0.20%
34.78%
47.01%
F
Conditioned medium
Zymosan-pHrodo intensity
BV2
BV2 + Cyt
BV2 + hiPSC-Astros-9429-3-A-med
BV2 + hiPSC-Astros-BJ-3-E-med
BV2 + hiPSC-Astros-553-SI-C-med
BV2 + hiPSC-Astros-2607-1-4-med
BV2 + pAstros-Cerebral cortex-1-med
BV2 + pAstros-Cerebral cortex-2-med

Figure S4. Related to Figure 4 | Impact of hiPSC-astrocytes on the phagocytic ability of BV2 microglial cells.

(**A**) Myelin is enriched after purification from brain (myelin prep) compared to whole brain homogenate (brain hom) as detected by western blotting. (**B, D, F**) Representative histograms used to quantify the values displayed in **Figure 4A, 4C, 4D** are shown in (**B**, **D**, **F**), respectively. Phagocytosing cells are marked as pHrodo+. (**C**) Phagocytic indices of BV2 cells, hiPSC-astrocytes and pAstrocytes incubated with 20 μg of pHrodo-labeled myelin or zymosan for 3 hours and analyzed by flow cytometry. Values were averaged from 4 to 8 different control hiPSC-Astrocytes and 2 to 4 different pAstrocytes. (**E**) Flow cytometry analysis of BV2 microglial cells and co-cultures of hiPSC-astrocytes and pAstrocytes with BV2 microglial cells stained with CD11b-APC and GFAP antibodies (n=5). Representative fluorescent intensity dot plots are shown. Data are representative of three independent experiments (n = 3) and shown as mean ± standard deviation. Treatment with 2 μM Cytochalasin D (Cyt) was used as a negative control for phagocytosis inhibition.

Table S1 | Screening results for the 11 initial astrocyte differentiation conditions.

Medium	Cell line	TUJ1	MAP2	GFAP	S100B	Cell condition and morphology	Subjective score for astrocyte differentiation
#1. Neuron	3651	+	+	-	-	Neuronal morphology	N.A
	4506	+	+	-	-		
#2. ScienCell	3651	+	-	+	+	Highly proliferative Astrocyte morphology	+++
	4506	+	-	+	+		
#3. Gibco	3651	+	-	-	-	Highly proliferative Resemble fibroblasts	-
	4506	+	+	+	+		
#4. Lonza	3651	+	-	+	+	Highly proliferative Astrocyte morphology	+++
	4506	+	-	+	+		
#5.	3651	+	-	+	+	Not proliferative Form spheres	+
	4506	+	-	+	+		
#6.	3651	+	-	-	-	Not proliferative Cell line variation	-
	4506	+	-	+	+		
#7.	3651	+	-	+	+	Not proliferative Astrocyte morphology	++
	4506	+	+	+	+		
#8.	3651	+	+	-	-	Cell death Not proliferative	-
	4506	+		+	+		
#9.	3651	+	-	-	-	Not proliferative Cell line variation	-
	4506	+		-	+		
#10.	3651	+	-	-	-	Cell line variation	+
	4506	+	+	-	+		
#11.	3651	+	-	+	+	Cell line variation	+
	4506	+	+	-	+		
#12.	3651	+	-	-	-	No astrocyte markers presence	-
	4506	+	+	-	-		

#1 is cortical neuron differentiation control and #2-12 are astrocyte differentiation conditions. Screening results from two cell lines evaluated by staining with a neuronal lineage marker, Class III β-tubulin (TUJ1), a neuronal marker, MAP2, astrocyte markers, GFAP and S100B, cell survival conditions and astrocyte-like morphologies.

Table S2 | Cell lines tested in each essay by four investigators.

			Astrocyte										NPC									
Cell line	Donor Sex	Grown by	IF		qRTPCR		FACS		IL-6 ELISA		RNAseq		IF		qRTPCR		FACS		IL-6 ELISA		RNAseq	
pAst Ctx	F	INV1	✓	INV3	✓	INV3	✓	INV4	✓	INV1	✓	INV1	N/A		N/A		N/A		N/A		N/A	
pAst Mb	M	INV1	✓	INV3	✓	INV3	✓	INV4	✓	INV1	✓	INV1	N/A		N/A		N/A		N/A		N/A	
pAst Cblm	F	INV1	✓	INV3	✓	INV3	✓	INV4	✓	INV1	✓	INV1	N/A		N/A		N/A		N/A		N/A	
pAst Mix	Unknown	INV1	✓	INV3	✓	INV3	✓	INV4	✓	INV1	x		N/A		N/A		N/A		N/A		N/A	
Total # of lines tested per assay			4		4		4		4		3											
9319-2-A	F	INV1	✓	INV1	✓	INV1	✓	INV4	✓	INV1	✓	INV1	✓	INV1	✓	INV1	✓	INV4	x		✓	INV1
3651-A-A	F	INV1	✓	INV1	✓	INV1	✓	INV4	✓	INV1	✓	INV1	✓	INV1	✓	INV1	✓	INV4	x		✓	INV1
9429-3-A	F	INV1	✓	INV1	✓	INV1	✓	INV4	✓	INV1	✓	INV1	✓	INV1	✓	INV1	✓	INV4	x		✓	INV1
BJ-3-E	M	INV1	✓	INV1	✓	INV1	✓	INV4	✓	INV1	✓	INV1	✓	INV1	✓	INV1	✓	INV4	x		✓	INV1
9319-2-A (2)	F	INV1	✓	INV1, 3	✓	INV1, 3	✓	INV4	✓	INV1	x		✓	INV1, 3	✓	INV1, 3	✓	INV4	✓	INV1	x	
3651-A-A (2)	F	INV1	✓	INV1, 3	✓	INV1, 3	✓	INV1	✓	INV1	x		✓	INV1, 3	✓	INV1, 3	✓	INV4	✓	INV1	✓	INV1
9429-3-A (2)	F	INV1	✓	INV1	✓	INV1	✓	INV1	✓	INV1	x		✓	INV1	✓	INV1	✓	INV4	x		✓	INV1
BJ-3-E (2)	M	INV1	✓	INV1	✓	INV1	✓	INV4	✓	INV1	x		✓	INV1	✓	INV1	✓	INV4	x		x	
F11350	M	INV3	✓	INV3	✓	INV3	✓	INV4	✓	INV1	x		✓	INV3	✓	INV3	✓	INV4	x		x	
F0510	M	INV3	✓	INV3	✓	INV3	✓	INV4	✓	INV1	x		✓	INV3	✓	INV3	✓	INV4	x		x	
2607-1-4	M	INV1	✓	INV3	✓	INV3	✓	INV4	✓	INV1	x		✓	INV3	✓	INV3	✓	INV4	x		x	
553-SI-C	M	INV1	✓	INV3	✓	INV3	✓	INV4	✓	INV1	x		✓	INV3	✓	INV3	✓	INV4	x		x	
3130-2-1	M	INV1	✓	INV3	✓	INV3	✓	INV4	✓	INV1	x		✓	INV3	✓	INV3	✓	INV4	x		x	
3113-3-2	F	INV1	x		x		✓	INV1	x		x		x		x		x		x		x	
3183-1-9	F	INV1	x		x		✓	INV1	x		x		x		x		x		x		x	
690-1-4	M	INV1	x		x		✓	INV1	x		x		x		x		x		x		x	
676-1-2	F	INV1	x		x		✓	INV1	x		x		x		x		x		x		x	
1442-4-3	M	INV1	x		x		✓	INV1	x		x		x		x		x		x		x	
2011-3-2	F	INV1	x		x		✓	INV1	x		x		x		x		x		x		x	
2620-B-4	M	INV1	x		x		✓	INV1	x		x		x		x		x		x		x	
2607-1-4 (2)	M	INV2	x		✓	INV3	✓	INV2	x		x		x		✓	INV3	x		x		x	
553-SI-C (2)	M	INV2	x		✓	INV3	✓	INV2	x		x		x		✓	INV3	x		x		x	
3113-3-2 (2)	F	INV2	x		✓	INV3	✓	INV2	x		x		x		✓	INV3	x		x		x	
690-1-4 (2)	M	INV2	x		✓	INV3	✓	INV2	x		x		x		✓	INV3	x		x		x	
676-1-2 (2)	F	INV2	x		x		✓	INV2	x		x		x		x		x		x		x	
1442-4-3 (2)	M	INV2	x		✓	INV3	✓	INV2	x		x		x		✓	INV3	x		x		x	
2620-B-4 (2)	M	INV2	x		✓	INV3	✓	INV2	x		x		x		✓	INV3	x		x		x	
2011-3-2 (2)	F	INV2	x		x		✓	INV2	x		x		x		x		x		x		x	
3130-2-3	M	INV2	x		✓	INV3	✓	INV2	x		x		x		✓	INV3	x		x		x	
499-5-2	M	INV2	x		x		✓	INV2	x		x		x		x		x		x		x	
581-1-2	M	INV2	x		✓	INV3	✓	INV2	x		x		x		✓	INV3	x		x		x	
1275-B-3	F	INV2	x		✓	INV3	✓	INV2	x		x		x		✓	INV3	x		x		x	
2476-1-4	F	INV2	x		✓	INV3	✓	INV2	x		x		x		✓	INV3	x		x		x	
2484-1-1	F	INV2	x		x		x		x		x		x		✓	INV2	x		x		x	
2962-2-1	M	INV2	x		x		x		x		x		x		✓	INV2	x		x		x	
2513-1-4	M	INV2	x		✓	INV3	✓	INV2	x		x		x		✓	INV3	x		x		x	
3121-1-4	F	INV2	x		x		✓	INV2	x		x		x		x		x		x		x	
3084-1-1	M	INV2	x		✓	INV3	✓	INV2	x		x		x		✓	INV3	x		x		x	
3158-4-1	F	INV2	x		✓	INV3	✓	INV2	x		x		x		✓	INV3	x		x		x	
3182-1-2	F	INV2	x		✓	INV3	✓	INV2	x		x		x		✓	INV3	x		x		x	
3183-1-4	F	INV2	x		✓	INV3	✓	INV2	x		x		x		✓	INV3	x		x		x	
3234-1-4	M	INV2	x		✓	INV3	✓	INV2	x		x		x		✓	INV3	x		x		x	
Total # of lines tested per assay			13		29		40		13		4		13		31		13		2		6	

INV, investigator 1-4, N/A, not applicable, check marks represent completed experiments, x marks represent experiment that have not performed.

Table S3 | qRT-PCR primer sequences.

GAPDH	Forward	AGGGCTGCTTTTAACTCTGGT
	Reverse	CCCCACTTGATTTTGGAGGGA
β-ACTIN	Forward	TGTCCCCCAACTTGAGATGT
	Reverse	TGTGCACTTTTATTCAACTGGTC
GFAP	Forward	GTCCCCCACCTAGTTTGCAG
	Reverse	TAGTCGTTGGCTTCGTGCTT
S100β	Forward	TGTAGACCCTAACCCGGAGG
	Reverse	TGCATGGATGAGGAACGCAT
VIM	Forward	TGGACCAGCTAACCAACGAC
	Reverse	GCCAGAGACGCATTGTCAAC
AQP4	Forward	GGCCGTAATCTGACTCCCAG
	Reverse	TGTGGGTCTGTCACTCATGC
ACSBG1	Forward	CCCCTTGACCTGTGATGACC
	Reverse	GAGACGGGATGGACTTGGA
APOE	Forward	GAGCAGGCCCAGCAGATAC
	Reverse	CTGCATGTCTTCCACCAGGG
βIII-TUBULIN	Forward	CCCGTTATCCCAGCTCCAATATGCT
	Reverse	ATGGCTTGACGTGCGTACTTCTCC
MAP2AB	Forward	AAACTGCTCTTCCGCTCAGACACC
	Reverse	GTTCACTTGGGCAGGTCTCCACAA
RELN	Forward	CATGATCAATGGGCTTTGGAC
	Reverse	GTATCGCCTAAGTGACCTTCG
CACNA1C	Forward	GAAGCGACAGAAGGACCG
	Reverse	CAAAAGGCCTAGGGAATGAGG

Table S4 | Genes included in the microfluidic cards.

Gene Symbol	Gene name	LifeTechnologies assay ID	RefSeq ID	Unigene ID
GAPDH	glyceraldehyde-3-phosphate dehydrogenase	Hs02758991_g1	NM_001256799.1	Hs.544577
18s RNA	eukaryotic 18s rRNA	Hs99999901_s1	NR_003286.2	-
SOX2	SRY (sex-determining region-Y)-box 2	Hs01053049_s1	NM_003106.3	Hs.518438
POU5F1	POU class 5 homeobox 1	Hs00999632_g1	NM_001173531.1	Hs.249184
LIN28A	lin-28 homolog A (C.elegans)	Hs00702808_s1	NM_024674.4	Hs.86154
NANOG	nanog homeobox	Hs04399610_g1	NM_024865.2	Hs.635882
NES	nestin	Hs04187831_g1	NM_006617.1	Hs.527971
FN1	fibronectin 1	Hs01549976_m1	NM_002026.2	Hs.203717
TUBB3	tubulin, beta 3 class III	Hs00801390_s1	NM_001197181.1	Hs.511743
FOXA2	forkhead box A2	Hs00232764_m1	NM_021784.4	Hs.155651
PAX6	paired box 6	Hs00240871_m1	NM_000280.4	Hs.270303
MAP2	microtubule-associated protein 2	Hs00258900_m1	NM_001039538.1	Hs.368281
RELN	reelin	Hs01022607_m1	NM_005045.3	Hs.655654
RBFOX3	RNA binding protein, fox-1 homolog (C.elegans) 3	Hs01370653_m1	NM_001082575.1	Hs.135229
ENO2	enolase 2 (gamma, neuronal)	Hs00157360_m1	NM_001975.2	Hs.511915
DLG4	discs, large homolog 4 (Drosophila)	Hs00176354_m1	NM_001128827.1	Hs.463928
CACNA1C	calcium channel, voltage-dependent, L-type, alpha 1C subunit	Hs00167681_m1	NM_000719.6	Hs.118262
GFAP	glial fibrillary acidic protein	Hs00909233_m1	NM_001131019.2	Hs.514227
VIM	vimentin	Hs00958111_m1	NM_003380.3	Hs.455493
S100B	s100 calcium binding protein B	Hs00902901_m1	NM_006272.2	Hs.422181
ALDH1L1	aldehyde dehydrogenase 1 family, member L1	Hs00201836_m1	NM_001270364.1	Hs.434435
ALDOC	aldolase C, fructose-biphosphate	Hs00902799_g1	NM_005165.2	Hs.155247
AIF1	allograft inflammatory factor 1	Hs00610419_g1	NM_001623.3	Hs.76364
ITGAM	integrin, alpha M (complement component 3 receptor 3 subunit)	Hs00355885_m1	NM_000632.3	Hs.172631

Table S5 | Proteome Profiler Human Cytokine Array.

Gene Symbol	Description
C5	Complement component 5
CD40LG	CD40 ligand
G-CSF	Granulocyte-colony stimulating factor
GM-CSF	Granulocyte-macrophage colony-stimulating factor
CCL1	Chemokine (C-C motif) ligand 1
CCL2/MCP-1	Chemokine (C-C motif) ligand 2
CCL3/MIP-1 alpha	Chemokine (C-C motif) ligand 3
CCL5/RANTES	Chemokine (C-C motif) ligand 5
CXCL1	Chemokine (C-X-C motif) ligand 1 (melanoma growth stimulating activity, alpha)
CXCL10/IP-10	Chemokine (C-X-C motif) ligand 10
CXCL11/I-TAC	Chemokine (C-X-C motif) ligand 11
CXCL12/SDF-1	Chemokine (C-X-C motif) ligand 12
ICAM-1	Intercellular Adhesion Molecule 1
IFN-gamma	Interferon, gamma
IL-1α	Interleukin 1 alpha
IL-1β	Interleukin 1 beta
IL-1ra	Interleukin 1 receptor antagonist
IL-2	Interleukin 2
IL-4	Interleukin 4
IL-5	Interleukin 5
IL-6	Interleukin 6
IL-8	Interleukin 8
IL-10	Interleukin 10
IL-12 p70	Interleukin 12
IL-13	Interleukin 13
IL-16	Interleukin 16
IL-17	Interleukin 17
IL-17E	Interleukin 17E
IL-18	Interleukin 18
IL-21	Interleukin 21
IL-27	Interleukin 27
IL-32α	Interleukin 32 alpha
MIF	Macrophage migration inhibitory factor (glycosylation-inhibiting factor)
Serpin E1/PAI-1	Serpin Family E Member 1/Plasminogen activator inhibitor-1
TNF-α	Tumor necrosis factor-alpha
TREM-1	Triggering receptor expressed on myeloid cells 1

SUPPLEMENTAL EXPERIMENTAL PROCEDURES

NPC-Astrocyte differentiation and culture

Forebrain NPCs were maintained at high density, grown on matrigel (BD Bioscience) in NPC medium (DMEM/F12 (Invitrogen: 10565), 1x N2 (Invitrogen: 17502-048), 1x B27-RA (Invitrogen: 12587-010)) and 20 ng/ml FGF2 (Invitrogen), resuspended in 1% BSA (Gibco) in PBS (Gibco)) and split approximately 1:3 every week with accutase (Millipore). NPCs could be expanded up to 14 passages. The quality of NPCs used for astrocyte differentiation is a critical variable in this protocol; careful quality control of NPC fate will increase the likelihood of a successful astrocyte differentiation. Low passage NPCs are frequently preferable. The astrocyte differentiation propensity of particularly intransient NPC lines can be improved by sorting for a CD271-/CD133+/CD184+ population by FACS (Cheng et al., 2017).

Forebrain NPCs were differentiated to astrocytes by seeding dissociated single cells at 15,000 cells/cm^2 density on matrigel-coated plates in astrocyte medium (ScienCell: 1801, astrocyte medium (1801-b), 2% fetal bovine serum (0010), astrocyte growth supplement (1852) and 10U/ml penicillin/streptomycin solution (0503)). Initial NPC seeding density and single cell dissociation are critical, particularly during the first 30 days of differentiation, in order to efficiently generate a homogenous population of astrocytes.

At day -1, after 5-10 min incubation with accutase at 37°C, NPCs were pipetted with a p1000 pipette 3-5 times, in order to yield a single cell suspension but limit cell death. Additional NPC medium was added and cells were transferred to a 15ml tube, spun at 500g for 5min, and plated on a matrigel-coated plate in NPC medium. At day 0, NPC medium was switched to astrocyte medium. From day 2, cells were fed every 48 hours for 20-30 days. When the cells reached 90-95% confluency (approximately every 6-7 days), they were split to the initial seeding density (15,000 cells/cm^2) as single cells in astrocyte medium, and cultured on matrigel, following 5-10 min incubation with accutase, pipetting, and washing with DMEM (Gibco).

After 30 days of differentiation, astrocytes could be split 1:3 every week with accutase and expanded up to 120 days (15-17 passages) in astrocyte medium containing 2% FBS. Following the initial 30-day differentiation period, astrocytes survive and expand for up to 30 days without FBS. All cell lines in the manuscript routinely tested negative for mycoplasma with MycoAlert PLUS mycoplasma detection kit (Lonza).

We caution that morphology and functional properties of hiPSC-astrocytes can change with increased passage (data not shown), which should be carefully recorded and matched in all experimental comparisons.

NPC differentiation from human iPSCs

hiPSCs were maintained in Human Embryonic Stem cell (HuES) medium (DMEM/F12 (Invitrogen), 20% KO-Serum Replacement (Invitrogen), 1x Glutamax (Invitrogen), 1x NEAA (Invitrogen), 1x 2-mercaptoethanol (Gibco), or complete mTeSR1 (StemCell Technologies) with 10 ng/ml StemBeads FGF2 (StemCultures) and differentiated to NPCs by either: 1) dual SMAD inhibition (0.1μM LDN193189 and 10μM SB431542) (Brennand et al., 2011) during embryoid body (EB) and rosette formation in EB medium (DMEM/F12 (Invitrogen: 10565), 1x N2 (Invitrogen: 17502-048), 1x B27-RA (Invitrogen: 12587-010)) or 2) Neural Induction Medium (StemCell Technologies). Rosette selection was performed after 14 days of culture by Rosette Selection Reagent (StemCell Technologies). NPCs were validated immunocytochemically

and/or by FACS using markers for SOX2 (Cell signaling: 3579S), PAX6 (Abcam: ab5790), FOXP2 (Abcam: ab16046) and NESTIN (Abcam: ab22035).

Generation of iNeurons from Human NPCs

NPCs were dissociated with accutase (Innovative Cell Technologies) and plated at 500,000 cells per well of a 24-well plate on day -2. Cells were plated on matrigel (BD Biosciences)-coated coverslips or plates in NPC medium (DMEM/F12/N2/B27/FGF2, Invitrogen). On day -1, h*NGN2* lentivirus (TetO-h*NGN2*-P2A-PuroR (Addgene: 79049) or TetO-h*NGN2*-P2A-eGFP-T2A-PuroR (Addgene: 79823)) together with CAGGs-rtTA lentivirus(Ho et al., 2015) at $1x10^6$ pfu/ml per plasmid (multiplicity of infection (MOI) of 2) was added in fresh NPC medium and spinfected at 1,000g for 1 hours. After 3-4 hours, the medium was replaced with fresh NPC medium. Doxycycline (2μg/l, Clontech) was added on day 0 to induce TetO gene expression and retained in the medium until the end of the experiment. On day 1, a 48 hr puromycin selection (1 μg/ml) period was started. On day 2, the culture medium was replaced by neuron medium: DMEM/F12 medium supplemented with N2/B27/Glutamax (Invitrogen) containing BDNF (20ng/ml, Peprotech), GDNF (10ng/ml, PeproTech), Dibutyryl cyclic-AMP (250μg/ml, Sigma), and L-ascorbic acid (200nM Sigma); Ara-C (2μg/l, Sigma) was added for 48 hours to the medium to inhibit proliferation of any non-neuronal cells. On day 4, hiPSC-derived astrocytes or primary astrocytes were seeded at 50,000 cells per well of the 24-well plate in the neuronal medium. FBS (2%) (Invitrogen) was added to the culture medium to support astrocyte viability. Beginning at day 4, half of the medium in each well was replaced every other day. h*NGN2*-induced neurons were assayed on day 17.

Flow Cytometry

Cells were dissociated using TryPLE (Gibco) or accutase (Millipore), fixed for 10 min in 4% paraformaldehyde (PFA), permeabilized and blocked with 0.5% (v/v) Triton (Sigma)/1% (w/v) bovine serum albumin (BSA, Sigma) in PBS and labeled with primary antibodies S100β (mouse, 1:200-1:1,000; Sigma-Aldrich: S2532), GFAP (chicken, 1:200-1:1,000; Aves Lab), GLAST/EAAT1 (rabbit, 1:100; BOSTER: PA2185), PAX6 (rabbit, 1:200; Abcam: ab5790), and NESTIN (mouse, 1:200; Abcam: ab22035) overnight at 4°C. Following 2 washes with 1 x PBS, the cell pellet was resuspended in blocking buffer with the appropriate Alexa Fluor 488, 568, or 647 conjugated secondary antibodies (1:200-1:1,000, Life Technologies) for 2hr at 4°C, then washed twice more with 1 x PBS, resuspended in FACS buffer (1 x PBS (no Mg2+/Ca2+)) and filtered using a 40 μm filter (BD Biosciences). Cytometry was performed using an LSR-II (BD Biosciences) and analysis was performed using Flowjo (v8.7.3, Treestar) or FCS Express 5 software (De Novo Software). Gating for positive cells was relative to a secondary antibody only control.

Immunocytochemistry

Cells were plated on acid-etched coverslips at 80,000-100,000 cells per well of a 24-well plate. Within 24hrs, astrocyte cultures were washed with PBS and fixed using 4% PFA (#15714, Electron Microscopy Sciences) for 20 min on ice, or 10% formalin solution (Sigma-Aldrich) for 15 minutes; washed 3 times with PBS 1X plus 0.01% Triton X-100 prior to pre-incubation with blocking solution made of PBS 1X plus 0.01% Triton X-100, and either 10% donkey serum or 1% bovine serum albumin (Sigma-Aldrich), for at least 1 hr. Cultures were then incubated in primary antibody solution overnight at 4˚C, followed by an incubation with secondary antibodies for 1-2hrs at room temperature. Primary antibodies used in this study were S100β (mouse, 1:1000; Sigma-Aldrich: S2532), GFAP (chicken, 1:2000; Aves Lab), Vimentin (rabbit, 1:500; Cell Signaling: R28#3932), b-III-tubulin (rabbit, 1:1000; Biolegend: 802001), polyclonal GLT1/EAAT2 and GLAST/EAAT1 (rabbit, 1:120, Life technology: PA5-34198), GLAST/EAAT1 (rabbit, 1:100;

BOSTER: PA2185), ALDH1L1 (rabbit, 1:250; Abcam: ab190298) PAX6 (rabbit, 1:200; Abcam: ab5790) NESTIN (mouse, 1:500; Abcam: ab22035), and Myelin Basic Protein (rabbit, 1:1000; Abcam:ab40390). Secondary antibodies used were Alexa Fluor 488, 568, or 647 conjugated (1:300, Life Technologies). Cultures were counterstained using 4',6-diamidino-2-phenylindole (DAPI, 1:1000-1:5000; Invitrogen: D1306). AquaPolymount mounting solution (#18606-20, Polysciences Inc.) was used to mount on coverslips. Coverslips were imaged with either a Zeiss LSM 780 microscope or Leica DMIL LED Inverted Routine Fluorescence Microscope.

RNA Expression studies for Quantitative Real Time PCR (qRT-PCR) and RNAseq

Cells were plated at 1,000,000 cells per well of a 6-well plate. Within 24-48 hrs, astrocyte cultures were washed with PBS and lysed with RLT buffer (Qiagen, # 74106) or Qiazol reagent (Qiagen). The total RNA was extracted from 30-day differentiated astrocytes with RNeasy mini kit (Qiagen, # 74106) with on-column DNaseI digestion (Qiagen, #79254) For standard qPCR, RNA was reverse transcribed into complementary DNA (cDNA) with iScript™ cDNA Synthesis kit (#1708890, Bio-Rad). cDNA was used as template for the quantitative PCR using a 7900 Real-Time PCR system (Applied Biosystems) with Power SYBR Green PCR Master Mix (Applied Biosystems). Gene expression was analyzed using the ΔΔCt method. qPCR results were normalized to GAPDH, β-actin and TBP (TATA-box binding protein) expression, and the values of uninduced fibroblasts were set to 1. Three replicates were used to determine the standard error. See the **Supplementary Table 3** for primer sequences.

For microfluidic card assays, RNA was reverse transcribed using the high capacity RNA to cDNA kit (LifeTechnologies). Individual channels on the cards were loaded with cDNA and Taqman® Universal Master Mix II (LifeTechnologies). The Taqman assays included in the microfluidic cards are listed in **Supplementary Table 4**. Gene expression was analyzed using the ΔΔCt method, and results were normalized to GAPDH and 18S ribosomal RNA. Gene expression fold changes were calculated compared to GAPDH expression. Each reaction was carried out in duplicate. The resulting data was subject to classical multidimensional scaling based on Euclidean distance in two dimensions, using R Studio (http://www.rstudio.com/). For RNAseq, RNA was quality controlled by BioAnalyzer (Agilent Technologies).

Analysis of RNA Sequencing Data

Paired-end RNA-seq data was generated using the Illumina HiSeq 2500 platform for hiPSC-astrocytes (n=4), neurons (n=6) and NPCs (n=8) (**Supplementary Table 5**), as well as for two primary astrocyte samples. Total RNA extracted from these samples was validated by qRT-PCR analysis before RNA sequencing. The paired-end sequencing reads were aligned to human hg19 genome using Star Aligner (version 2.5.0b). Following read alignment, FeatureCounts(Liao et al., 2014) was used to quantify gene expression at the gene level based on Ensembl gene model GRCh37.70. The gene level read counts data was normalized as counts per million (CPM) using the trimmed mean of M-values normalization (TMM) method(Robinson et al., 2010) to adjust for sequencing library size difference. To control for potential sex differences in gene expression, sex effects were corrected by linear regression. Multi-dimensional scaling (MDS) and cluster analysis were performed using the R programming language. Differential gene expression between different cell types was predicted by linear model analysis using the Bioconductor package limma(Ritchie et al., 2015). For differential expression between hiPSC-derived astrocytes and NPCs/neurons, a paired comparison was performed to account for matched genotypes. To adjust for multiple tests, the false discovery rate (FDR) of the differential expression test was estimated using the Benjamini–Hochberg (BH) method(Vasudevan et al.)·(Benjamini and Hochberg, 1995). Genes with FDR < 0.05 and log2 fold change > 1 or < -1 were considered significant.

Meta-analysis of brain cell type specific RNAseq data from Zhang *et al* 2016
We downloaded the raw RNAseq data of multiple brain cell types(Zhang et al., 2016) from gene expression omnibus (accession GSE73721) and then processed the sequencing reads using the same star-FeatureCounts pipeline as described above. The gene level read counts were combined with the data generated in this project. The merged data was normalized using the TMM approach and then corrected for sex and batch using linear regression. Hierarchical cluster analysis was performed using R.

Functional enrichment analysis
For functional enrichment analysis of differential expression gene signatures, the gene ontology (GO) annotations, and canonical pathways (Biocarta, KEGG and Reactome) gene sets were obtained from the Molecular Signatures Database (MSigDB) v4.0(Subramanian et al., 2005). Enrichment analysis was carried out using the Fisher's exact test assuming the sets of genes were identically independently sampled from the genome-wide genes profiled. The BH approach was employed to constrain the FDR.

IL-6 ELISA, Multi-Analyte ELISArray and protein array
hiPSC-derived astrocytes and primary human fetal astrocytes were seeded at 200,000viable cells per well of a 24-well plate in astrocyte medium one day before the experiment. Cells were treated for 24 hours with 50 ng/ml or 100 ng/ml of Poly(I:C) (InvivoGen, #tlrl-pic), 10 µg/ml or 50 µg/ml of Lipopolysachharide (LPS) (Sigma-Aldrich, #L5886), or 5 μM or 10 μM of human beta amyloid, Aβ42 (CaliforniaPeptide, #641-15) and vehicle control solutions (Saline for Poly(I:C) and LPS or Tris-HCl, pH 7.5 for Aβ42). The medium from astrocyte-enriched cultures was collected, centrifuged at 21,000g for 5 min at 4˚C and stored at -20˚C or proceeded assays.

Samples from all experiments were processed in parallel; comparisons were made within ELISA plates but not between them. Samples were analyzed with an IL-6 ELISA assay (Affymetrix eBioscience, #88-7066) and Human Inflammatory Cytokines Multi-Analyte ELISArray (Qiagen, #MEH-004A), according to manufacturer's guidelines. Absorbance at 450 nm was measured by spectrophotometry and was quantified at 450 nm, using 570 nm as a reference wavelength. Gene expression profiles were analyzed by RT2 Profiler PCR Arrays (Qiagen). Proteome Profiler™ Human Cytokine Array (R&D Systems, #ARY005B) was used according to manufacturer's guidelines. Proteome profiler intensity dot blots were quantified using Gimp2.8 software and were normalized to mean intensities of reference spots.

Phagocytosis assay
BV2 mouse microglial cell line was maintained in DMEM (Gibco, 11965) supplemented with 5% FBS (Sigma, F4135) and 1:100 Pen Strep (Gibco, 15140). To analyze the influence of astrocyte-secreted factors on the phagocytic activity of BV2 microglia, hiPSC-derived astrocytes and primary human fetal astrocytes were plated at approximately 1 million cells per well in a 6-well plate and allowed to grow for 2 weeks prior to medium conditioning. Astrocyte conditioned medium (ACM) was collected after 2 days of incubation and centrifuged at 21,000g for 5min at 4 ˚C. BV2 cells were seeded at 200,000 cells per well in a 24-well plate and allowed to attach for 8 to 9 hours. Cells were washed once with PBS and treated with ACM from hiPSC-derived astrocyte and primary astrocyte cultures. BV2 cells incubated with fresh astrocyte medium were used as a control. Zymosan conjugated with a pHrodo red dye (Thermo Fisher, P35364) was dissolved in PBS at 1 mg/ml and sonicated for 10 minutes. After 20 hours of incubation with ACM, BV2 cells were washed with PBS once and further incubated with 30 µg of pHrodo-labeled for 3 hours. Cells were trypsinized, washed with PBS once and resuspended in 500 µl of 1% BSA in PBS. Cells were kept on ice and immediately analyzed by flow cytometry.

To analyze the phagocytic ability of hiPSC-derived astrocytes and primary astrocytes in comparison with BV2, cells were seeded at 120,000 cells per well in a 24-well plate and allowed to reach confluency. Cells were incubated with 20 μg of pHrodo-labeled myelin for 3 hours. Myelin was prepared from the wild type mouse brain as described in(Jahn et al., 2008), and labeled with red pHrodo dye according to the manufacturer's instructions (Thermo Fisher, P36600). After incubation cells were gently collected in accutase, washed with PBS and resuspended in 1% BSA in PBS. Uptake of pHrodo was immediately analyzed with flow cytometry.

To analyze the effect of astrocyte co-culture on the phagocytic ability of BV2 cells, hiPSC-derived astrocytes and primary astrocytes were seeded at 120,000 cells per well in a 24-well plate. Cells were allowed to reach confluency, when BV2 cells were seeded on top of astrocytes at 150,000 cells per well. After 24 hours the co-culture was treated with 30 μg of pHrodo-labeled zymosan for 3 hours, and collected in 1% BSA in PBS as described before for immediate analysis by flow cytometry.

For the analysis of cell populations in co-culture and their contribution to phagocytosis, incubation with pHrodo-labeled zymosan was followed by sample collection with trypsinization and further blocking in 2% BSA in PBS for 30 minutes on ice. Cells were surface-labeled with CD11b-APC (eBiosciences) 1:100 in 1% BSA in PBS for 1 hour on ice. For intracellular labeling cells were washed and fixed with 2% paraformaldehyde for 30 minutes on ice, then washed with PBS once and incubated with GFAP antibody 1:100 for 1 hour on ice. After a wash in PBS, cells were incubated with the secondary antibody 1:100 conjugated to AlexaFluor488 for 30 minutes on ice and prepared for flow cytometry analysis by a wash in PBS and resuspension in 1% BSA in PBS. At least 30,000 events were collected in each flow cytometry analysis. Cells were gated on an FSC-A / SSC-A dot plot to exclude cell debris, additional gating on an FSC-A / FSC-W dot plot was used to exclude doublets. Isotype control and secondary antibody only labeling were used to define the gates for cells positive for CD11b or GFAP labeling. Single labeling of co-cultured cells with pHrodo-labeled zymosan, CD11b-APC and GFAP were used to set up compensation between channels. Cells pre-treated with 2μM Cytochalasin D for 30 minutes before and during the incubation with pHrodo-labeled zymosan were used as a negative control for phagocytic ability of BV2 and to define the population of phagocytosing cells.

All flow cytometry data were acquired on a LSRII (BD Biosciences) and analyzed using FCS Express 5 software (De Novo Software). Phagocytic index was calculated for pHrodo+ population as follows: % of gated cells was multiplied by geometric mean fluorescence intensity of pHrodo and then divided by 10^6 for presentation.

Spontaneous calcium transient imaging

Calcium imaging analysis was performed on hiPSC-derived astrocytes or human primary astrocytes from cerebral cortex region (ScienCell) on acid-etched glass coverslips. Cells were incubated for 15 min at room temperature with 2 μM Fluo-4-AM (Invitrogen, F-14201) and 0.02% Pluronic F127 in Krebs HEPES buffer (KHB) (10 mM HEPES, 4.2 mM $NaHCO_3$, 10 mM dextrose, 1.18 mM $MgCl_2.6H_2O$, 1.18 mM $KH2PO_4$, 4.69 mM KCl, 118 mM NaCl, 1.29 mM $CaCl_2$, pH7.3), then washed three times with KHB and allowed to recover for 5 minutes in KHB. Time-lapse images (40x water-immersion objective; NA = 0.8) were acquired on the green channel (DM:485; BA:495-540HQ) at 1.16 s intervals (0.9 Hz) on an Olympus FV1000 MPE Microscope using a 473 nm laser (Olympus LD473nm (15mW)). Cells were imaged for 348 s under continuous perfusion with gravity-fed KHB. A single glutamate (3 μM) in KHB pulse was applied for 35 s beginning at ~ 35 s. We imaged an area of 380 μm^2 for multiple coverslips originating from 4 different hiPSC-astrocyte lines and 3 different primary astrocytes

preparations. For peak analysis, ROIs were first identified by automated segmentation of time-averaged images of image stacks using FluoroSNNAP (Patel et al., 2015) Fluorescence signal from the identified ROIs was then quantified by calculating mean pixel intensity values on the same program. Fluorescent traces were exported and then analyzed with custom Matlab routines that calculated the number and amplitude of Ca^{2+} spikes and percentage of spontaneously active cells. In peak detection, 50 RFU was taken as the minimum amplitude for a peak based on visual inspection of multiple recordings.

Statistical analysis

For all experiments, data are represented as mean ± SD or SEM of three to five biological replicates. Statistical significance was determined using a two-tailed homoscedastic Student's t-test or one-way ANOVA and Dunnett's post-hoc test for differences of means between each group and a control group of data with parametric distribution. Significant comparisons are labeled with * $p < 0.05$, ** $p < 0.01$, *** $p < 0.001$.

SUPPLEMENTAL REFERENCES

Benjamini, Y., and Hochberg, Y. (1995). Controlling the False Discovery Rate: A Practical and Powerful Approach to Multiple Testing. Journal of the Royal Statistical Society Series B (Methodological) *57*, 289-300.

Brennand, K.J., Simone, A., Jou, J., Gelboin-Burkhart, C., Tran, N., Sangar, S., Li, Y., Mu, Y., Chen, G., Yu, D*., et al.* (2011). Modelling schizophrenia using human induced pluripotent stem cells. Nature *473*, 221-225.

Cheng, C., Fass, D.M., Folz-Donahue, K., MacDonald, M.E., and Haggarty, S.J. (2017). Highly Expandable Human iPS Cell-Derived Neural Progenitor Cells (NPC) and Neurons for Central Nervous System Disease Modeling and High-Throughput Screening. Current protocols in human genetics *92*, 21 28 21-21 28 21.

Ho, S.M., Hartley, B.J., Tcw, J., Beaumont, M., Stafford, K., Slesinger, P.A., and Brennand, K.J. (2015). Rapid Ngn2-induction of excitatory neurons from hiPSC-derived neural progenitor cells. Methods.

Jahn, O., Tenzer, S., Bartsch, N., Patzig, J., and Werner, H.B. (2008). Myelin Proteome Analysis: Methods and Implications for the Myelin Cytoskeleton. Neuromethods *79*, 171–236.

Liao, Y., Smyth, G.K., and Shi, W. (2014). featureCounts: an efficient general purpose program for assigning sequence reads to genomic features. Bioinformatics *30*, 923-930.

Patel, T.P., Man, K., Firestein, B.L., and Meaney, D.F. (2015). Automated quantification of neuronal networks and single-cell calcium dynamics using calcium imaging. J Neurosci Methods *243*, 26-38.

Ritchie, M.E., Phipson, B., Wu, D., Hu, Y., Law, C.W., Shi, W., and Smyth, G.K. (2015). limma powers differential expression analyses for RNA-sequencing and microarray studies. Nucleic Acids Research *43*, e47.

Robinson, M.D., McCarthy, D.J., and Smyth, G.K. (2010). edgeR: a Bioconductor package for differential expression analysis of digital gene expression data. Bioinformatics *26*, 139-140.

Subramanian, A., Tamayo, P., Mootha, V.K., Mukherjee, S., Ebert, B.L., Gillette, M.A., Paulovich, A., Pomeroy, S.L., Golub, T.R., Lander, E.S*., et al.* (2005). Gene set enrichment analysis: A knowledge-based approach for interpreting genome-wide expression profiles. Proceedings of the National Academy of Sciences of the United States of America *102*, 15545-15550.

Vasudevan, B., Ashish, B., Amitabh, S., and A, P.M. (2010). Primary Cutaneous Histoplasmosis in a HIV-Positive Individual. Journal of global infectious diseases *2*, 112-115.

Zamanian, J.L., Xu, L., Foo, L.C., Nouri, N., Zhou, L., Giffard, R.G., and Barres, B.A. (2012). Genomic analysis of reactive astrogliosis. J Neurosci *32*, 6391-6410.

Zhang, Y., Sloan, S.A., Clarke, L.E., Caneda, C., Plaza, C.A., Blumenthal, P.D., Vogel, H., Steinberg, G.K., Edwards, M.S., Li, G*., et al.* (2016). Purification and Characterization of Progenitor and Mature Human Astrocytes Reveals Transcriptional and Functional Differences with Mouse. Neuron *89*, 37-53.